eLife

Reviewed Preprint
v1 • February 19, 2025
Not revised

Reviewed Preprint
v2 • April 9, 2026
Revised by authors

For correspondence:
oguzhan.baltaci@petermac.org
ben.hogan@petermac.org

Competing interests: No competing interests declared

Funding: See page 23

Reviewing editor: Benoit Vanhollebeke, Université Libre de Bruxelles, Belgium

Mural cells protect the adult brain from hemorrhage but do not control the blood-brain barrier in developing zebrafish

Oguzhan F Baltaci[1,2], Andrea Usseglio Gaudi[1,2], Stefanie Dudczig[1,2], Weili Wang[3], Scott Paterson[1,2], Maria Cristina Rondon-Galeano[1,2], Ye-Wheen Lim[3], James Rae[3], Anne Lagendijk[3], Robert G Parton[3,6], Alison Farley[1,2,4], Benjamin M Hogan[1,2,5]

[1]Organogenesis and Cancer Program, Peter MacCallum Cancer Centre, Melbourne, Australia • [2]Sir Peter MacCallum Department of Oncology, University of Melbourne, Melbourne, Australia • [3]Institute for Molecular Bioscience, The University of Queensland, St Lucia, Australia • [4]Walter and Eliza Hall Institute of Medical Research, Melbourne, Australia • [5]Department of Anatomy and Physiology, University of Melbourne, Melbourne, Australia • [6]Centre for Microscopy and Microanalysis, The University of Queensland, St Lucia, Australia

eLife Assessment

This **important** study addresses the contribution of pericytes to the organization and permeability control of the zebrafish blood-brain barrier (BBB). By analyzing pdgfrb mutant zebrafish that lack brain pericytes, the authors reveal that the resulting cerebrovascular network is abnormally patterned. Remarkably, however, the barrier retains its restrictive permeability during larval and juvenile stages. More pronounced vascular defects become evident in adults, where localized BBB leakage coincides with hemorrhages and aneurysm formation. Based on **convincing** and beautifully documented imaging data, the authors argue that, unlike what has been reported in rodent systems, pdgfrb-dependent pericytes are not essential for maintaining BBB integrity in the zebrafish brain.

https://doi.org/10.7554/eLife.104061.2.sa3

Abstract

The blood-brain barrier (BBB) protects the brain from circulating metabolites and plays central roles in neurological diseases. Endothelial cells (ECs) of the BBB are enwrapped by mural cells including pericytes and vascular smooth muscle cells (vSMCs) that regulate angiogenesis, vessel stability and barrier function. To explore mural cell control of the BBB, we investigated neurovascular phenotypes in zebrafish *pdgfrb* mutants that lack brain pericytes and vSMCs. As expected, mutants showed an altered cerebrovascular network with mispatterned capillaries. Unexpectedly, mutants displayed no BBB leakage at larval stages of development. This demonstrates that pericytes and vSMCs do not control BBB function in developing zebrafish. Instead, we observed juvenile and adult BBB disruption occurring at "hotspot" focal hemorrhages at large vessel aneurysms. ECs at leakage hotspots showed induction of caveolae on abluminal surfaces and structural defects including basement membrane thickening and disruption. Our work suggests that capillary pericytes regulate cerebrovascular patterning in development and vSMCs of major arteries protect from hemorrhage and BBB breakdown in older zebrafish. The fact that young zebrafish have a functional BBB in the absence of mural cells calls for renewed interrogation of mural cell control of the BBB throughout vertebrate evolution.

Introduction

Mammalian neurovascular endothelial cells (ECs) have unique functional and structural properties to regulate substance exchange between the blood and the brain, establishing the blood-brain barrier (BBB)[1,2]. Loss of normal BBB function is associated with neuropathological states, including neurodegeneration, infection and cancer[1,2]. Mural cells are vascular support cells that include pericytes and vascular smooth muscle cells (vSMCs) and control vascular development, function and BBB permeability[3–9]. PDGFB/PDGFRβ signaling is required for the development of mural cells[3,4,10–12] and their depletion in PDGFB- or PDGFRβ-deficient rodents causes altered angiogenesis, aneurysm and vessel leakiness[3–6,13]. Strikingly, rodent models of pericyte loss have an open BBB, with free transport of tracer dyes from the blood stream into the brain parenchyma but an otherwise intact vasculature[5,6]. These and other observations have led to a current model whereby pericytes control BBB function by suppressing EC transcytosis, via a mechanism not yet fully understood. Such a mechanism holds significant translational promise to safely "open" the BBB in therapeutic settings, by discovering ways to disrupt pericyte control of ECs[5,14].

Studies of the BBB using invertebrates like *Drosophila* and some basal vertebrate fishes (e.g. some *Elasmobranchii* and *Chondrostei*) have suggested that the makeup of the BBB can vary significantly across the phylogeny. These species display a primarily glial cell barrier, rather than an EC barrier[15,16]. However, in the modern teleost *Danio rerio* (zebrafish) the BBB cellular composition is more similar to that seen in mammals[17–21]. As in mammals, the zebrafish BBB is controlled by tightly adherent vascular ECs that share many characteristics with the ECs of the mammalian brain. Zebrafish BBB endothelium expresses conserved molecular markers (e.g. *glut1*, *cldn5*, *mfsd2a*)[18,20–23] and displays similar tight cell-cell junctions as observed at the mammalian BBB[17,20,22]. The membrane transport protein Mfsd2a has been suggested to have a conserved role in control of BBB function in zebrafish and mice[21,24], likely acting to reduce the transfer of substances between bloodstream and parenchyma by suppressing EC transcytosis[25,26]. Furthermore, during development the mechanisms that control the formation of BBB ECs appear to show a high level of conservation between zebrafish and mice. Recent studies have identified major roles for Wnt–β-catenin signaling, brain EC specific MMPs, Vegfs and chemokine signaling in early BBB vascular EC development[23,27–29].

After the initial development of zebrafish BBB vasculature, mural cell populations develop and mature. Transcriptionally, developing pericytes and vSMCs express many genes that are highly conserved with mammals, for example zebrafish pericytes express well known markers such as *pdgfrb*, *kcne4* and *abcc9* [30]. As in mice, *pdgfrb* mutants fail to form brain pericytes, exhibit loss of vSMCs and display aneurysms as adults[13,31]. As well as conserved *pdgfrb* control of mural cell development, Notch signaling[32] also plays a role in mural cell development in zebrafish and in mice, with Notch 1 and 3 controlling the formation of pericytes in mice and Notch 2 and Notch 3 paralogues important in zebrafish[33,34]. Overall, studies have suggested a high level of conservation of the molecular control of mural cell development, yet how mural cells control BBB function has not been interrogated in detail in zebrafish.

BBB function is first established in zebrafish between 3 days post fertilization (dpf, no barrier) and 5 dpf (established barrier)[21]. During this period, developing mural cells (pericytes and vSMCs) are establishing and expanding their interactions with brain ECs[31,34,35]. The first glial cell neurovascular interactions are also observed during this period[36]. Throughout subsequent larval, juvenile and adult development vSMC, pericyte and glial cell coverage of the vasculature increases[31,36,37]. This is similar to mammals, albeit with some differences in the relative timing that lineages arise, and the percentage of coverage of neurovasculature by pericytes and glia may be lower in zebrafish. In mammals, microglia are known to play important roles in the control of the BBB and neurovascular unit[38]. Zebrafish have a microglial/macrophage population, but it is yet to be explored in detail in the control of the BBB[39–41] and differences in other innate immune cells in the CNS has been recently reported[42].

Overall, while there are some areas remaining to be fully explored, the development, cellular composition and the central role of ECs in the control of the zebrafish BBB is very similar to mammals. As such, zebrafish are accepted as a highly accessible model to study BBB function, as well as mural cell control of the BBB, relevant to mammalian biology[19].

Here, we explored mural cell control of BBB function in zebrafish. We used *pdgfrb* mutants with loss of both pericytes and vSMCs, coupled with carefully optimized intravascular tracer dye injections. We analyzed barrier function from developmental to adult stages and found that at larval stages up to 14 dpf, well after the establishment of the BBB, loss of mural cells does not lead to measurable BBB leakage or loss of BBB integrity. In adult animals, we observed loss of BBB integrity that was consistent with leakage at hotspots, found to be aneurysm associated hemorrhages. These hotspots were also observed in juvenile animals (1 month old) and appeared to increase in number as animals aged. Our observations provide no definitive evidence of BBB leakage at capillary networks that might be consistent with a broad increase in EC transcytosis or loss of barrier integrity independent of focal hemorrhages. This work demonstrates that young animals can have a functional BBB in the absence of mural cells and highlights the central role for the EC in control of barrier function across the zebrafish neurovasculature.

Results

To investigate the influence of mural cells upon the neurovasculature, we generated a *pdgfrb* mutant (*pdgfrb*^{uq30bh}, hereafter *pdgfrb*$^{-/-}$), which possesses an early deletion leading to a frameshift, predicted to cause a premature stop codon and a putative null allele (Extended Data Fig. 1a). Using both the *TgBAC(pdgfrb:EGFP)*^{uq15bh} and *TgBAC(abcc9:abcc9-T2A-mCherry)*^{um139} transgenic marker strains, we observed that pericytes were lost in the cerebral central arteries of *pdgfrb* mutants (Fig. 1a, Extended Data Fig. 1b–c), as observed in previous studies[13,31]. These mutants showed indistinguishable development from their wild-type siblings up to 30 days post fertilization (dpf) and progressively reduced survival and craniofacial defects thereafter (Extended Data Fig. 1d–f), consistent with previous studies of *pdgfrb* null loss-of-function mutants[13,35]. To assess how brain vasculature develops without pericytes, we imaged, traced and quantified central arteries in the midbrain (Fig. 1a–c). At 7 dpf, mutants displayed significantly reduced vascular complexity compared to siblings, with reduced vessel length and branch points (Fig. 1d–e). This was more severe at 14 dpf, demonstrating the phenotype is progressive (Fig. 1d–e). Timecourse imaging revealed the reduction in vascular complexity was apparent from 5 dpf (Fig. 1f–g). These results suggest that the pericytes (as vSMCs mature after 5 dpf[34]) regulate cerebral angiogenesis or remodeling from early in larval development.

We next tested BBB function in mutants at 7 and 14 dpf. We performed intravenous injection of fluorescently conjugated tracers of various molecular weights (1-kDa NHS, 10- and 70-kDa Dextran), and live imaged fish at 2 hours post injection (hpi, the same timing used in[21]) (Extended Data Fig. 2a). 2000-kDa Dextran was co-injected to normalize for the amount of vascular tracer delivered in each animal, and we measured intravascular versus extravascular tracer intensity to assess leakage (see methods for full details). In control animals, quantification confirmed that 2000-kDa tracer remained stably within the vasculature, while 1 kDa and 10 kDa were more readily detected in the brain parenchyma and 70 kDa provided intermediate sensitivity (Extended Data Fig. 2b–c). This validated the use of 2000-kDa tracer to normalize for amount of tracer injected, as reported elsewhere[43]. To provide additional confidence in our measurements, we also normalized the extravasated tracer intensity to the EC marker *kdrl* (*Tg(kdrl:EGFP)*^{s843} *or Tg(kdrl:Hsa.HRAS-mCherry)*^{s916}). We found no evidence of elevated 10- or 70-kDa Dextran tracer extravasation into the brain parenchyma of *pdgfrb* mutants compared to siblings at either timepoint (7 or 14 dpf) using any of our normalization methods (Fig. 2a–d, Extended Data Fig. 3a–d). To confirm that our quantification methods were sufficiently sensitive to detect BBB leakage, we assessed 10- and 70-kDa tracer leakage before and after the establishment of BBB function (at 3 and 7 dpf[21]). With both 10- and 70-kDa tracers, we could detect an open BBB at 3 dpf

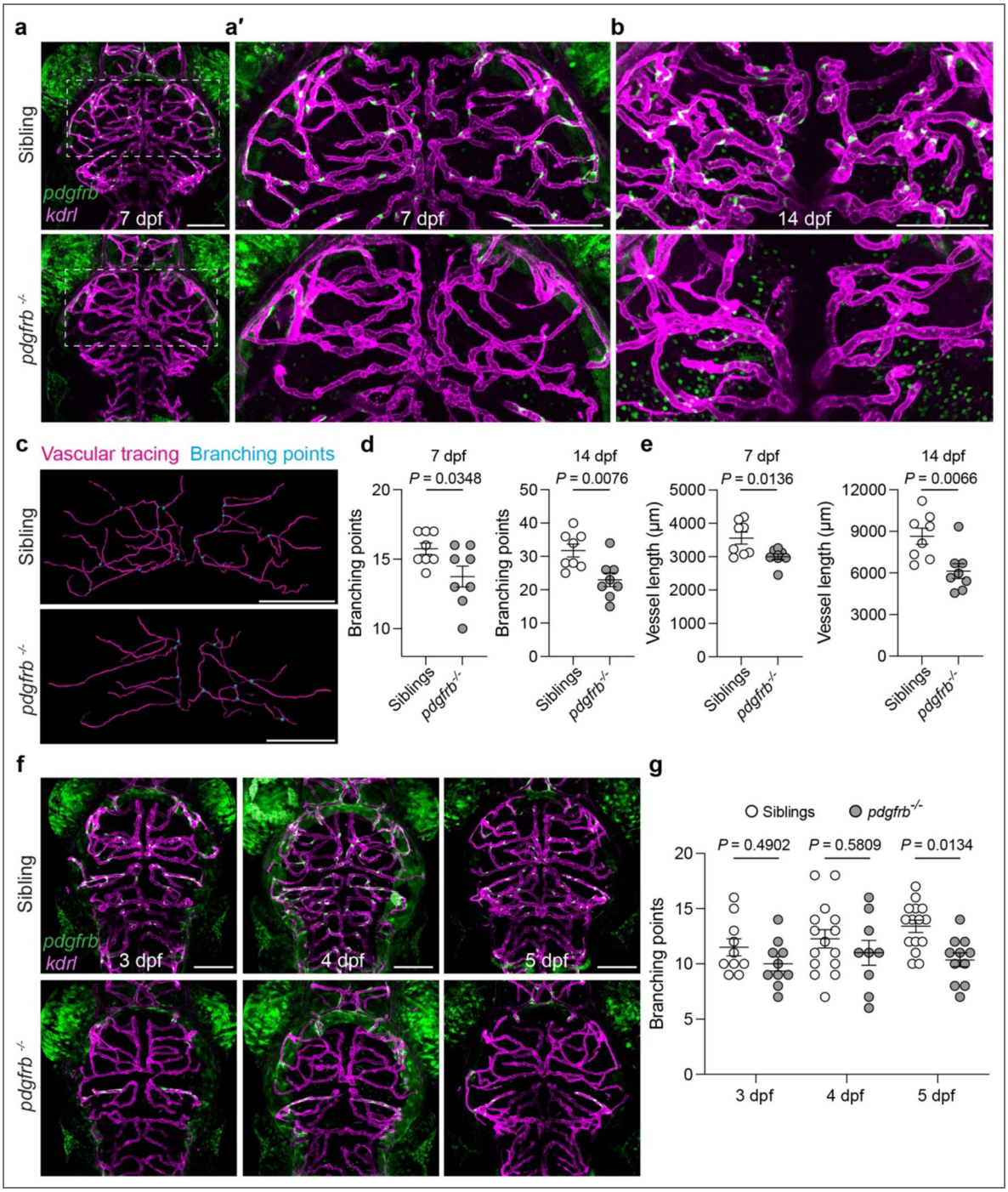

Fig. 1. Mural cell-deficient larval brain vasculature displays abnormal patterning.

a–b Maximum intensity projections of mural cells (*TgBAC(pdgfrb:EGFP)*^{uq15bh}) and brain vasculature (*Tg(kdrl:Hsa.HRAS-mCherry)*^{s916}) in siblings and *pdgfrb* mutants at 7 (**a**) and 14 dpf (**b**). (**a'**) shows enlarged view of the white box in (**a**) highlighting the midbrain central arteries. **c**, Representative images of vascular tracing at 7 dpf using Imaris 10.1. Lumenized blood vessels branching from the middle mesencephalic central arteries in the midbrain were traced. **d–e**, Quantification of midbrain branching points (**d**) and vessel length (**e**). Data are mean±SEM, n=8 per group, unpaired *t*-tests. **f**, Maximum intensity projections of mural cells (*TgBAC(pdgfrb:EGFP)*^{uq15bh}) and brain vasculature (*Tg(kdrl:Hsa.HRAS-mCherry)*^{s916}) in siblings and *pdgfrb* mutants at 3-5 dpf. **g**, Quantification of branching points of midbrain central arteries demonstrating the first detectable vessel patterning phenotype at 5 dpf. Data are mean±SEM, n=10 per group at 3 dpf, n=15 sibling and 9 *pdgfrb*$^{-/-}$ at 4 dpf, n=15 sibling and 11 *pdgfrb*$^{-/-}$ at 5 dpf, two-way analysis of variance (ANOVA) followed by multiple comparisons with Tukey's correction. **a**, **a'**, **b**, **c**, **f**, Dorsal views, anterior up, scale bars: 100 µm.

that was closed at 7 dpf (Fig. 2e–f). Together, these results show that we can accurately measure BBB leakage and integrity in zebrafish and that based on these measures neither pericytes nor vSMCs are necessary for BBB function during larval stages.

To investigate how mural cells control cerebral vasculature at later stages of life, we tissue-cleared brains of adult stage *pdgfrb* mutants and siblings[44] and performed whole brain imaging. We confirmed loss of pericytes and vSMCs at this stage using *TgBAC(pdgfrb:EGFP)*^{uq15bh} and *TgBAC(acta2:EGFP)*^{uq17bh} (Fig. 3a–b). We examined a consistent region of the left optic tectum (midbrain) and detected decreased branching of capillaries and increased diameter of major vessels (Fig. 3d–f). The observed vessel dilation was restricted to larger caliber arteries that would normally be invested with vSMCs (Extended Data Fig. 4a–b) and was not seen in capillaries in this region of the brain (Fig. 3e–f). The loss of vSMCs was observable from the earliest stages of vSMC development and artery dilation was observed by 21 dpf, consistent with previous studies[13] (Fig. 3c, Extended Data Fig. 4c–d). This suggests that major vessel dilation seen in *pdgfrb* mutants is due to loss of vSMCs and that reduced branching of capillaries is due to loss of pericytes (given the timing observed in Fig. 1).

To investigate BBB integrity at later stages, we injected 3-month-old adult zebrafish with 10-kDa Dextran. Brightfield imaging of vibratome-sectioned brains revealed severe aneurysms across large caliber vessels (Fig. 4a) with blood pooling that was potentially consistent with vessel ruptures (Fig. 4c) as previously reported[35]. Furthermore, we detected parenchymal accumulation of tracer dye closely associated with large caliber vessel aneurysms (Fig. 4b–c). To quantify the distribution of parenchymal tracer dye from deep (around major artery aneurysms) to superficial (capillary beds) brain regions, we measured fluorescence intensity in 10 brain regions approximately 100 microns apart from medial to lateral locations. This demonstrated accumulation of tracer dye in medial regions associated with aneurysm in mutants (Fig. 4d–e). These animals showed little evidence of leakage in capillary beds, with marginally higher tracer intensity in mutants than controls in lateral locations that could be due to diffusion from medial locations with high concentrations of tracer (Fig. 4e). To better understand this extravasated tracer accumulation, we conducted whole brain imaging after tracer injection in 5-month-old adults. Interestingly, we observed highly localized 70-kDa tracer accumulation in regions that could be considered leakage "hotspots" at large caliber vessel aneurysms (Fig. 5a; Supplementary Videos 1 and 2).

As 10-kDa tracer showed higher sensitivity than 70-kDa tracer in our control experiments (Extended Data Fig. 2b–c), we examined 10-kDa tracer injections at earlier stages and found that hotspots were readily detectable from as early as 1 month using this lower molecular weight tracer (Fig. 5b). The hotspots were not readily detectable using 70-kDa Dextran in 2-month-old zebrafish, consistent with increased sensitivity of 10-kDa tracers (Extended Data Fig. 5a–d). Interestingly, the quantification of hotspots in whole cleared brains at 1 and 5 months of age showed that the number increased with aging, suggesting a progressive loss of BBB integrity at focal sites of leakage (Fig. 5c). To further understand the nature of leakage hotspots, we examined red blood cells in *pdgfrb* loss-of-function adults. We used *pdgfrb* Crispant knockouts, which we validated by finding that F0 CRISPR consistently reproduced the adult mutant phenotype (Extended Data Fig. 5e–f). Using the *Tg(gata1:DsRed)*^{sd2} transgenic line to label erythrocytes, together with tracer injection, we found that knockout animals showed tracer accumulation concomitant with extravasated red blood cells at hotspots (Fig. 5d). This identified hotspots as sites of focal hemorrhage. Notably, these sites were not detected at capillaries (Fig. 5e). Taken together, this shows that as mutants age, loss of BBB integrity is associated with an increasing number of hotspot sites of focal hemorrhage, that are found along aneurysmal vessels.

The quantification of tracer dye intensity at 2 hpi in adult mutants from medial (major vessels) to lateral (capillaries) locations indicated leakage most closely associated with hotspot focal hemorrhages. However, the intensity of tracer dye found in the lateral capillary regions was measurably higher than in control animals (Fig. 4e). To test if this was likely due to progressive diffusion of tracers from medial to lateral locations or if there may be some local leakage at capillaries, we examined 10-kDa tracer leakage at 0.5 and 6 hpi. While hotspots could be detected

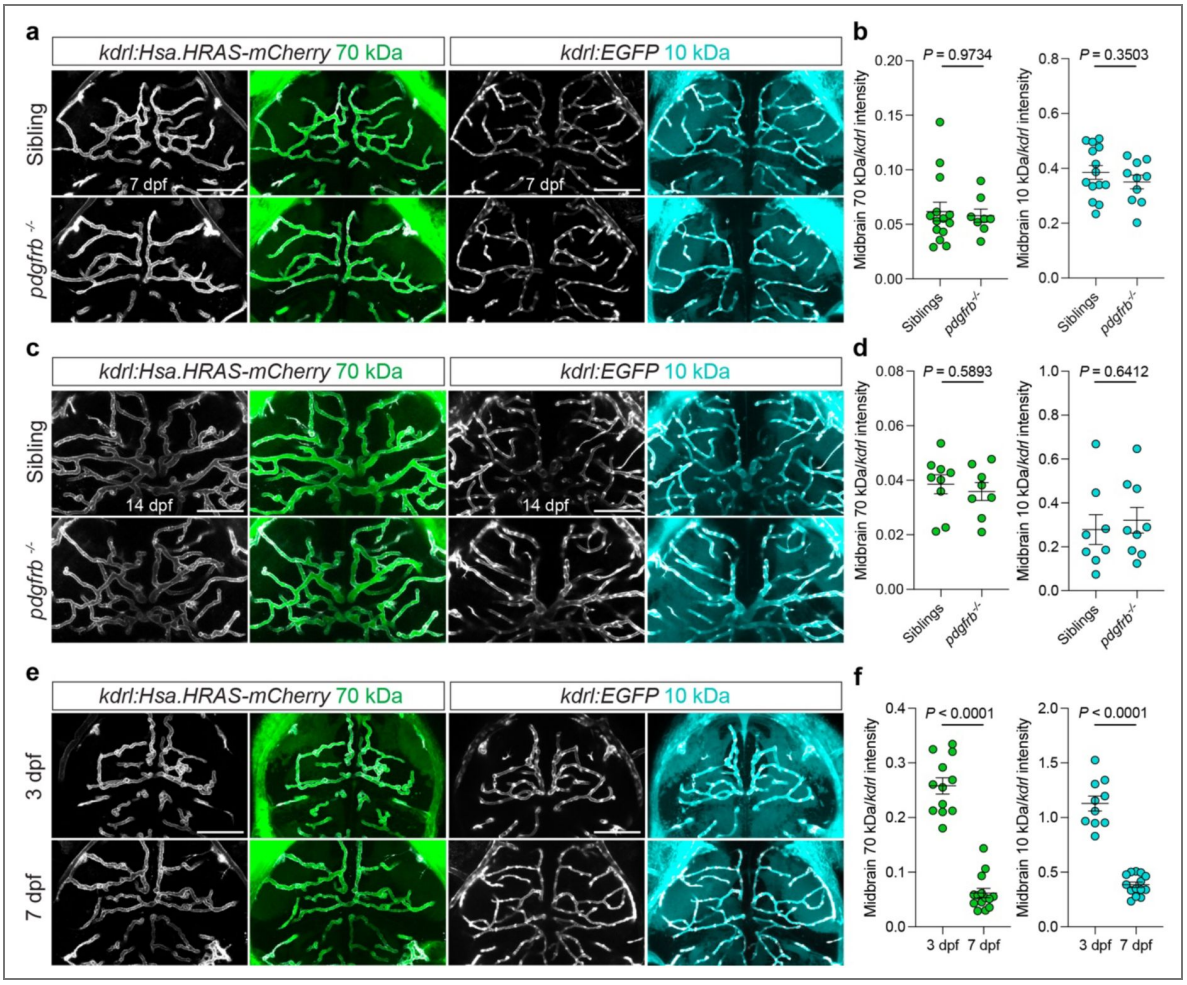

Fig. 2. BBB integrity is maintained in *pdgfrb* mutants during larval stages.

a, **c**, **e**, Fluorescent tracer leakage assays in the midbrain of zebrafish larvae using 70 kDa Dextran–Fluorescein or 10 kDa Dextran–Alexa Fluor™ 647, visualised with vascular reporters (gray) *Tg(kdrl:Hsa.HRAS-mCherry)*^{s916} and *Tg(kdrl:EGFP)*^{s843}. Siblings and *pdgfrb* mutants at 7 dpf (**a**) and 14 dpf (**c**) show no differences in tracer extravasation. Wild-type larvae at 3 and 7 dpf (**e**) serve as a positive control, illustrating reduced tracer leakage by 7 dpf. Dorsal views, anterior up, scale bars: 100 µm. **b**, **d**, **f**, Quantification of midbrain parenchymal 70- and 10-kDa dextran fluorescence intensity normalized to vascular *kdrl* reporter intensity. Data are mean±SEM. At 7 dpf (**b**): n=14 siblings and 8 *pdgfrb*$^{-/-}$ for 70 kDa, and n=14 siblings and 10 *pdgfrb*$^{-/-}$ for 10 kDa. At 14 dpf (**d**): n=9 siblings and 8 *pdgfrb*$^{-/-}$ for 70 kDa, and n=8 siblings and 9 *pdgfrb*$^{-/-}$ for 10 kDa. For the positive control at 3 and 7 dpf (**f**): n=12 (3 dpf) and 14 (7 dpf) for 70 kDa, and n=10 (3 dpf) and 14 (7 dpf) for 10 kDa. Unpaired t-tests for 10 kDa dextran comparisons at 3 vs 7 dpf and for sibling vs *pdgfrb*$^{-/-}$ comparisons at 7 and 14 dpf, and for 70-kDa dextran at 14 dpf. Mann–Whitney U tests for 70-kDa dextran comparisons at 3 vs 7 dpf and for sibling vs *pdgfrb*$^{-/-}$ comparisons at 7 dpf due to non-normal data distribution.

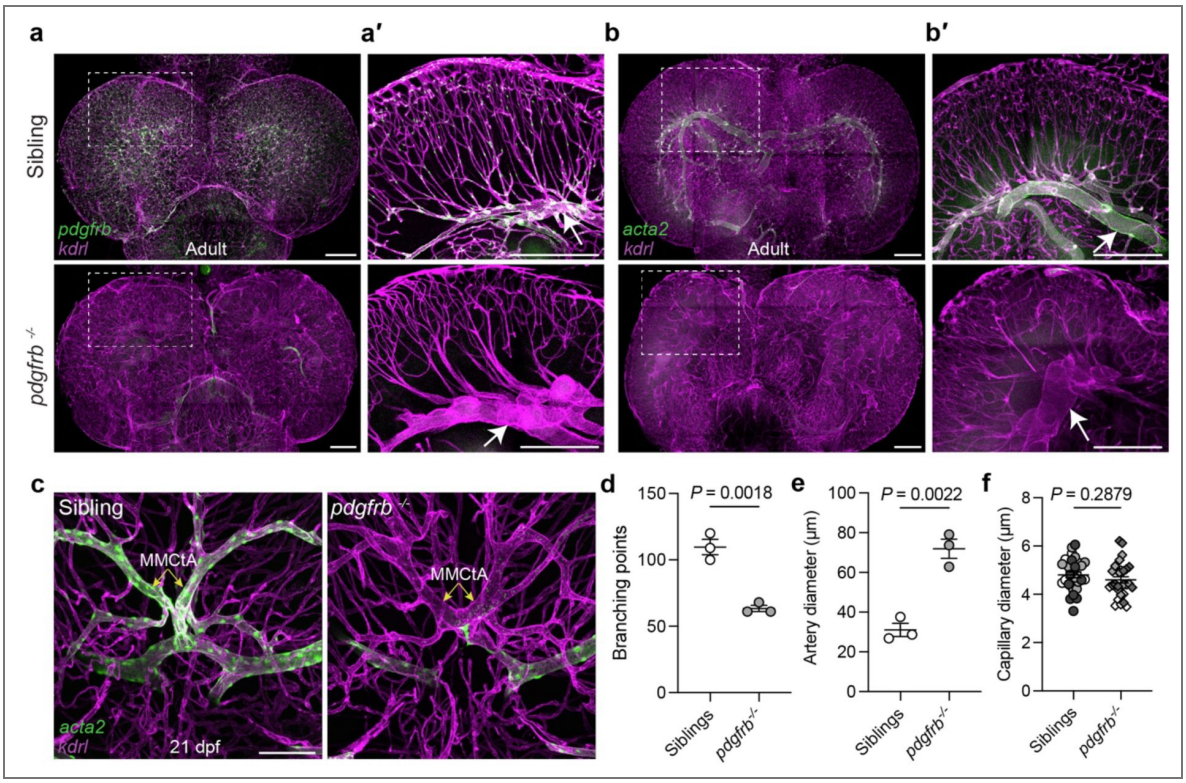

Fig. 3. Adult *pdgfrb* mutants lack mural cells and display dilated arteries.

a, **b**, Confocal projections of whole brain imaging in siblings and *pdgfrb* mutants at 5 months of age, showing brain vasculature using *Tg(kdrl:Hsa.HRAS-mCherry)*^{s916} and mural cells using *TgBAC(pdgfrb:EGFP)*^{uq15bh} (**a**) as a global marker and *TgBAC(acta2:EGFP)*^{uq17bh} (**b**) as a vSMC marker. Dorsal views, anterior up, scale bars: 250 µm. **a'**, **b'**, Subset of z-slices from the whole brain imaging in (**a**) and (**b**) (white boxes) indicating mural cell loss and abnormal capillary network patterning. 100-µm-thick maximum intensity projections (MIP) were generated using the continuation of the left middle mesencephalic central artery (MMCtA, arrow) as an anatomical landmark. Scale bars: 250 µm. **c**, Confocal projections from whole brain imaging in sibling and *pdgfrb* mutants at 21 dpf. Siblings show *acta2:EGFP*-positive vSMC coverage along MMCtAs (yellow arrows). *pdgfrb* mutants have dilated MMCtAs with absent vSMCs. Scale bar: 100 µm. **d–f**, Quantification of capillary branching points (**d**), artery diameter (**e**) and capillary diameter (**f**) using the area shown in (**a'**). Data are mean±SEM, n=3 animals per group. Artery diameter was quantified by averaging 5 points per animal, and capillary diameter was quantified by measuring 10 capillary diameter per animal. Each animal marked with a different color in **f**. Unpaired t-tests for branching points and artery diameter, nested t-test for capillary diameter.

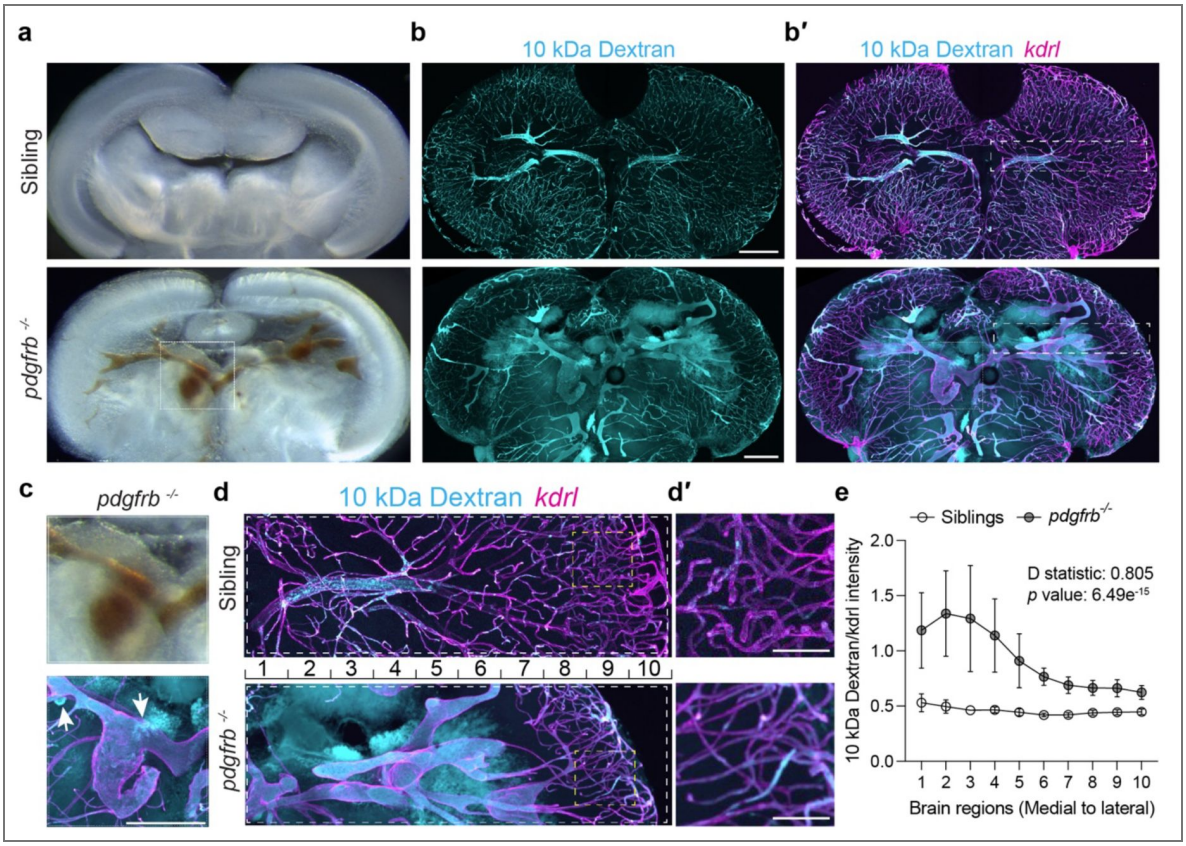

Fig. 4. Adult *pdgfrb* mutants display aneurysms and vascular integrity defects.

a, Representative images of coronal midbrain sections obtained from 3-month-old sibling and *pdgfrb* mutants. **b**, Fluorescent tracer leakage assays in 3-month-old siblings and *pdgfrb* mutants (2 hpi). 10 kDa Dextran–Cascade Blue (**b**) was used to assess extravasation, and *Tg(kdrl:Hsa.HRAS-mCherry)*^{s916} was used to label the brain vasculature (merge in **b'**). Scale bar: 250 µm. **c–c'**, Enlarged regions from (**a**) and (**b'**) (dotted box) displaying blood and tracer accumulation (arrows) in *pdgfrb* mutants. Scale bar: 250 µm. **d**, Enlarged regions from (**b**) (dashed box) displaying vasculature and tracer leakage from medial (arterial region) to lateral (capillary region) regions. Area was divided into 10 regions (~100 µm intervals) for quantification. **d'**, Enlarged view of yellow box in (**d**) showing capillary beds with intravascular tracer.Scale bar: 50 µm. **e**, Quantification of parenchymal 10 kDa tracer intensity (medial to lateral) normalized to vascular *kdrl* intensity. Data are mean±SEM, each point represents average normalized tracer intensity per brain region, n=5 sibling and 4 *pdgfrb*$^{-/-}$, two-sample Kolmogorov–Smirnov test.

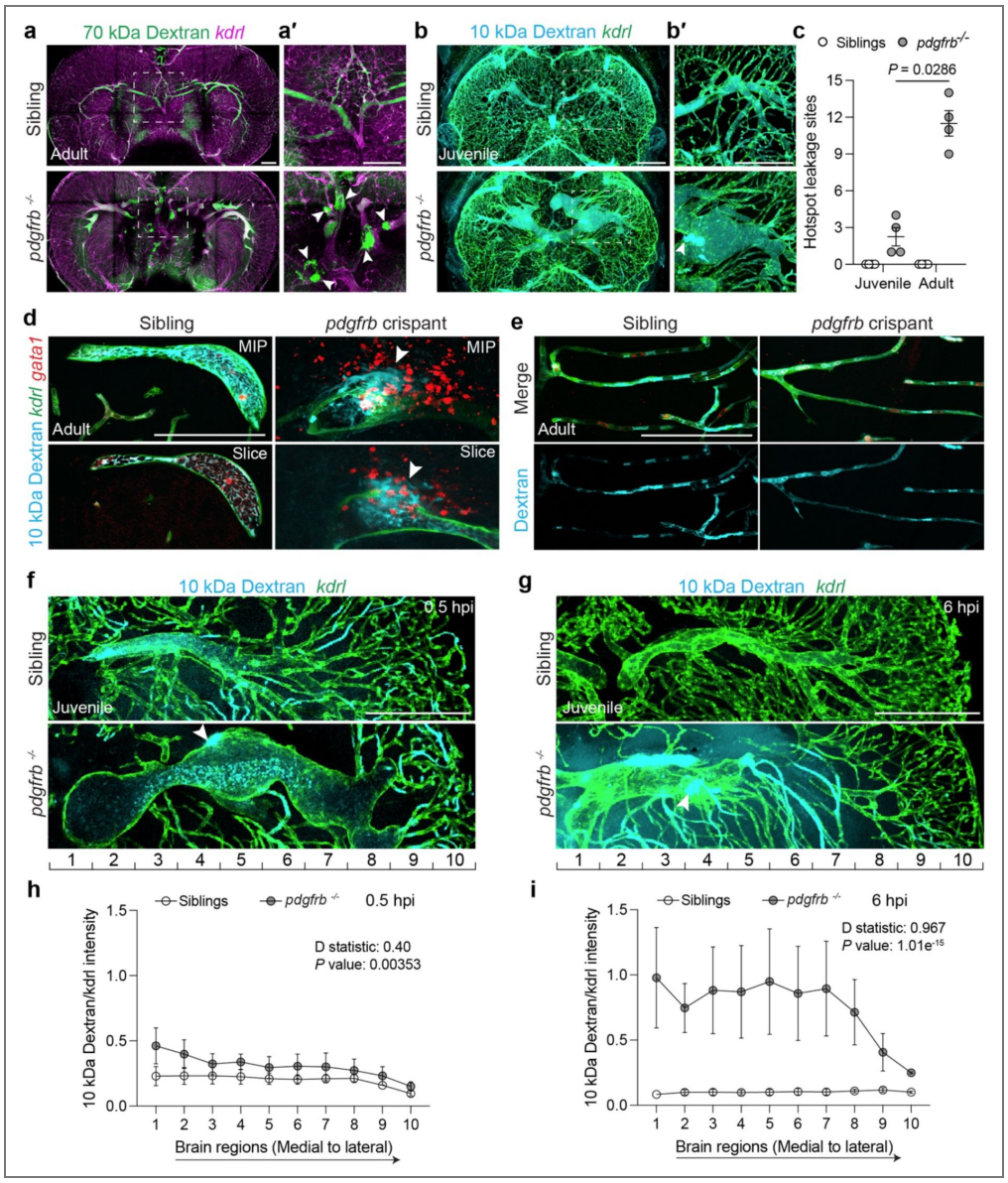

Fig. 5. Adult and juvenile *pdgfrb* mutants display vessel rupture and tracer accumulation at aneurysm hotspots.

a–a', Fluorescent tracer leakage assays in 5-month-old sibling and *pdgfrb* mutants. 70 kDa Dextran–Fluorescein was detected outside the vessels marked by *Tg(kdrl:Hsa.HRAS-mCherry)*^{s916} at aneurysm hotspots (arrowheads) shown in white box (magnified in **a'**). **b–b'**, Fluorescent tracer leakage assays in 1-month-old sibling and *pdgfrb* mutants. 10 kDa Dextran–Alexa Fluor™ 647 was detected outside the vessels marked by *Tg(kdrl:EGFP)*^{s843} at aneurysm hotspots (arrowhead) shown in white box (magnified in (**b'**)). **a–b**, Brains were collected at 2 hpi, dorsal views, anterior is up, scale bars: 200 µm. **c**, Quantification of hotspot leakage sites per animal in the midbrain region showing increased numbers in older animals. Data are mean±SEM, n=4 per group, unpaired t-test. **d–e**, High resolution imaging of artery (**d**) and capillary zones (**e**) in brain regions of 10-week-old adult *pdgfrb* crispants and uninjected siblings after tracer injection (2 hpi). 10 kDa Dextran–Alexa Fluor™ 647 injected, blood vessels (*Tg(kdrl:EGFP)*^{s843}) and red blood cells (*Tg(gata1:DsRed)*^{sd2}) are shown in MIPs and single Z-sections. Arrowheads indicate examples of hotspots. Capillary zones shown in MIPs (all channels) and single 10-kDa Dextran channel lack hotspots. Scale bar: 100 µm. **f–g**, Fluorescent tracer leakage assays in 1-month-old sibling and *pdgfrb* mutants shown in confocal projections of coronal midbrain sections collected at 0.5 hpi (**f**) or 6 hpi (**g**). 10 kDa Dextran–Alexa Fluor™ 647 was used to assess extravasation, and *Tg(kdrl:EGFP)*^{s843} was used to label the brain vasculature. The area was divided into 10 regions (~70 µm intervals) for quantification (see Extended Data Fig. 6 for full section image). Arrowheads indicate examples of hotspots. Scale bar: 200 µm. **h–i**, Quantification of parenchymal 10-kDa dextran intensity (medial to lateral) normalized to vascular *kdrl* intensity. Data are mean±SEM, each point represents average normalized tracer intensity per brain region, n=3 sibling and 5 *pdgfrb*$^{-/-}$ for 0.5 hpi, and n=3 per group for 6 hpi, two-sample Kolmogorov–Smirnov test.

at 0.5 hpi, we detected little tracer accumulation in medial locations and no evidence of parenchymal tracer leakage at lateral capillary locations (Fig. 5f, h, Extended Data Fig. 6a–a''). However, after 6 hours of diffusion of tracer within the brain, we clearly observed tracer at both medial and lateral locations, with higher intensity in medial locations (Fig. 5g, i, Extended Data Fig. 6b–b''). While we cannot rule out the possibility of slow leakage of tracer at capillaries occurring concurrently with leakage at hemorrhages, these observations seem consistent with a primary source of leakage at focal hemorrhages, followed by diffusion of tracer throughout the parenchyma.

Pericytes are proposed to regulate the BBB by suppressing transcytosis through brain capillary ECs[5,6]. This model is built on the observation by electron microscopy of the induction of increased numbers of vesicular structures and caveolae in leaky pericyte-deficient vessels[5,6]. To investigate if the loss of BBB integrity is associated with ultrastructural changes, we performed electron microscopy. We imaged large caliber vessels and capillaries (Fig. 6a–b, Extended Data Fig. 7a) and examined cellular junctions, basement membrane and caveolae (defined as uncoated vesicular profiles of <100 nm diameter). While tight junctions between endothelial cells remained intact, caveolae numbers along large vessel aneurysms in *pdgfrb* mutants were significantly increased (Fig. 6a''–c). This increase was almost exclusive to the abluminal side of the ECs (Fig. 6c). This abluminal accumulation of caveolae may be more associated with changes in the mechanical state of ECs (as caveolae are highly regulated by membrane tension[45,46]) than changes in intracellular transport. Furthermore, we detected thickening of basement membrane (BM) (Fig. 6d), gaps in the BM and fluid accumulation outside the vessel wall at aneurysms in mutants. We found no obvious difference in the caveolae density in capillary ECs of *pdgfrb* mutants compared with siblings (Extended Data Fig. 7b). Thus, leakage hotspots at aneurysms are associated with a loss of the normal flattened morphology of ECs, caveola induction and disruption of the BM, all factors that could contribute to or be observed concurrent with vessel wall rupture.

Discussion

Brain vasculature is endowed with mural cells that control vascular development and stability[3,4,13,47]. Studies in rodents have shown that pericytes regulate BBB integrity, with knockout of *Pdgfb* or *Pdgfrb* leading to vessel dilations and brain hemorrhages from early in development[3,4]. However, hypomorphic mutant alleles impacting *Pdgfb* or *Pdgfrb* show increased leakage of the BBB, with the severity of the leakage phenotype correlating with the expressivity of the pericyte phenotype[5,6]. BBB leakage is associated with increased vesicular structures in ECs and the "open" BBB state in the absence of mural cells is thought to be caused by hotspots of increased EC transcytosis[2,48]. Other potentially relevant pathways in ECs that could be altered by pericytes include altered cell-cell adhesion (e.g. Cldn5[14]), control of Mfsd2a[21,26], Netrin1-Unc5B signaling[49] or vitronectin regulation of integrin receptors[50], but direct links are yet to be established. Some studies using other models to deplete pericytes in mice have reported loss of pericytes without vessel leakage. For example, optical or chemical ablation of pericytes in the brain or retina of mice can be achieved without compromising the integrity of BBB or blood-retinal barrier[51,52], however these methods may induce inflammatory or compensatory mechanisms that also influence local vasculature. Taken together, these studies show that mural cells and in particular pericytes control the BBB in mammals, yet the precise downstream mechanisms by which pericytes regulate EC function require further study.

We show using zebrafish that mural cells are involved in cerebrovascular patterning in larval and juvenile animals, but these vessels maintain BBB function in the absence of mural cells. While the zebrafish BBB has been shown to be established between 3 and 5 dpf, we find that our leakage assays at 7 and 14 dpf in mural cell-deficient *pdgfrb* mutants indicate intact BBB function and wildtype vessel integrity. This is unlikely to be due to technical issues with detecting leakage, as multiple measures and methods of tracer normalization produced consistent results. Furthermore, we can readily detect the "open" BBB before it closes during development (Fig. 2e–f). This demonstrates that a functional vertebrate BBB can exist in the absence of pericytes. Importantly, while other species have a glial cell BBB (e.g. *Drosophila*, some sharks and sturgeon), the zebrafish

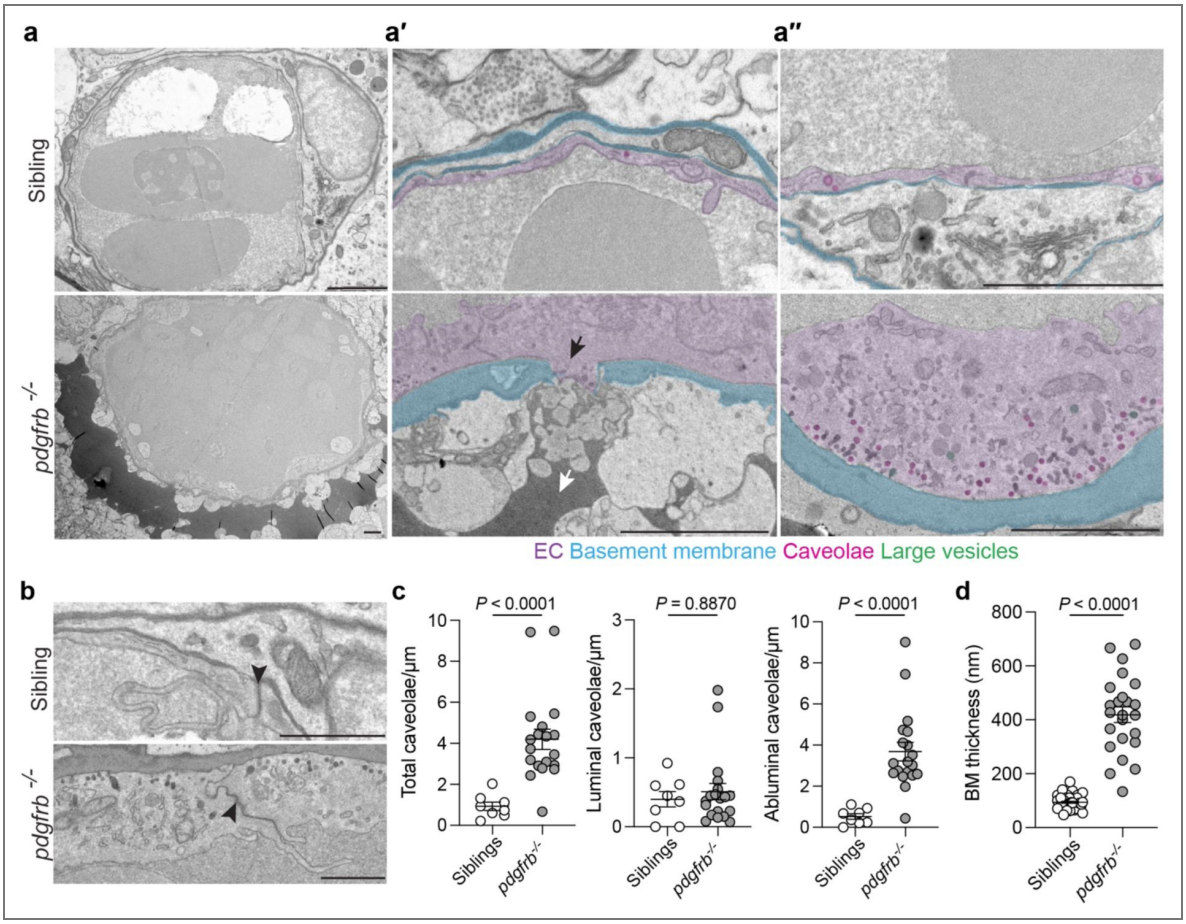

Fig. 6. Adult *pdgfrb* mutants display structural endothelial cell defects and vessel rupture.

a–a'', Transmission electron microscopy images of sectioned adult zebrafish brain vessels at 5 months of age. *pdgfrb* mutants show basement membrane thickening and breakdown (black arrow), serum accumulation outside the vessels (white arrow) (**a'**), increased abluminal endothelial caveolae (**a''**). Pseudocolors shown are ECs (purple), basement membrane (cyan), caveolae (magenta) and vesicles larger than 100 nm (green). Scale bars: 2 µm. **b**, Magnified regions from (**a**) showing intact tight junctions (arrowheads) in both siblings and *pdgfrb* mutants. Scale bars: 1 µm. **c**, Quantification of endothelial caveolae. Caveolae were defined as uncoated spherical profiles <100 nm in diameter and scored as luminal or abluminal (see methods for details). Measurements were made for n=3 vessels for each group and a total of 8 different cellular regions measured for siblings and 19 for mutants. Data are mean±SEM and are not distributed normally, Mann–Whitney U test was applied. **d**, Quantification of basement membrane thickness, which was scored in 6 different regions per vessel with n=8 vessels in siblings 4 in *pdgfrb* mutants across n=3 animal per group. Data are mean±SEM, unpaired t-test. Data are mean±SEM and are not distributed normally, Mann–Whitney U test was applied.

is well established to have an EC barrier and the glial cell coverage at the stages analyzed here is far from complete[36], making glial cell compensation for a loss of pericytes unlikely. There are other evolutionary differences (e.g. developmental timing, innate immune differences[42,53]) between zebrafish and mammals and our observation of intact BBB function without mural cells could represent an additional divergence. However, the high level of conservation of developmental pathways in BBB ECs and the very similar transcriptional signatures of both neurovascular ECs and mural cells between species[19,30,34,54] may make this surprising. Once additional mechanisms of pericyte-EC crosstalk are established in mice and zebrafish, deeper mechanistic comparative studies will help to better understand if our observations identify major differences in BBB control between these organisms or not.

Ultimately, in older mutants from 1 month of age onwards, BBB integrity defects are observable with major arteries progressively harboring aneurysms and focal hemorrhages (leakage hotspots). These aneurysms are likely due to the loss of vSMCs seen in our *pdgfrb* mutants and other zebrafish *pdgfrb* mutant models[13,35]. Adult mutant hotspots show extravascular erythrocytes and tracer dye, demonstrating that focal hemorrhages are a cause of vessel leakage. Similar to this, in *Pdgfb* or *Pdgfrb* mutant mice with strong phenotypic expressivity, hemorrhages are also reported (although not in mild or hypomorphic mutants used in BBB studies)[3,4,12]. These observations suggest a highly conserved role for mural cells in the regulation of aneurysm and hemorrhage in mice and zebrafish. In our zebrafish model, BBB leakage in juvenile and adult animals appears to only be observed once hemorrhages or hotspots are present. Coupled with the fact that larval zebrafish can have no mural cells, but intact barrier function, we suggest that any roles for mural cells in BBB integrity beyond control of aneurysm and hemorrhage are likely to be minor roles in this setting. It remains possible that there is slow undetectable capillary leakage, but future models that specifically lack capillary pericytes and not vSMCs will be needed to test this. Understanding the nature of hotspot leakage more broadly in various mammalian and non-mammalian models of mural cell deficiency would seem likely to uncover further insights into BBB regulation. Deeper understanding of the fundamental biology of the BBB is still needed and will pave the way for increasingly sophisticated efforts to target the BBB in disease in the future.

Methods

Zebrafish husbandry

Zebrafish work was conducted in compliance with animal ethics committees at the Peter MacCallum Cancer Centre, The University of Melbourne and The University of Queensland. The following previously published transgenic lines were used in this study: *TgBAC(pdgfrb:EGFP)*^{uq15bh} [55], *Tg(kdrl:Hsa.HRAS-mCherry)*^{s916} [56], *Tg(kdrl:EGFP)*^{s843} [57], *Tg(gata1:DsRed)*^{sd2} [58], *TgBAC(acta2:EGFP)*^{uq17bh} [55], and *Tg(5xUAS:RFP)*^{nkuasrfp1a} [59].

To ensure optical transparency, live imaging was performed in *slc45a2* (ENSDARG00000002593) F0 knockout animals as previously described[60] or by adding 0.003% 1-phenyl-2-thiourea (PTU) to embryo water at 1-day post-fertilization (dpf).

BAC recombineering and transgenesis

The *TgBAC(abcc9:abcc9-T2A-mCherry)*^{uom139} transgenic line was generated by BAC recombineering as previously described[61,62]. Briefly, T2A-mCherry insert with a kanamycin cassette was amplified by PCR using *pCS2-T2A-mCherry-KanR* plasmid as template. The primers used for amplifying the insert were:

5'-atggagcaggaggacggcctgtttgcatcttttgtcaaagccgacatgGAGGGCAGAGGAAGTCTGCTA-3'

5'- aaaatggcttttattgatctgttaaggccaaaagtggtgtaaagtggggaTCAGAAGAACTCGTCAAGAAGGCG-3'
(lowercase letters indicate homology arms to the BAC vector; uppercase letters indicate primer binding sites on the template plasmid).

The amplified insert was introduced into *CH211-58C15* (*abcc9*) BAC clone containing a pRedET plasmid (GeneBridge, Heidelberg, Germany) and iTol2 cassette. Approximately 1 nL of purified BAC DNAs (100 ng/μL) mixed with *tol2* transposase mRNA (25 ng/μL) were injected into single-cell stage embryos. Injected fish were raised to adulthood and screened by fluorescence and PCR for germline transmission. The *pdgfrb:gal4FF* BAC construct was generated previously[31] and was injected to produce the *TgBAC(pdgfrb:gal4FF)*^{um140} transgenic line. The *pdgfrb:gal4FF* BAC construct was kindly provided by Dr. Nathan Lawson (Department of Molecular, Cell, and Cancer Biology, University of Massachusetts Chan Medical School, USA).

Genome editing and genotyping

The *pdgfrb*^{uq30bh} mutant strain was generated using CRISPR/Cas9-mediated genome editing. The resulting allele carries a 39-bp deletion and a 5-bp insertion in exon 3 of *pdgfrb* (ENSDARG00000100897), leading to a predicted frameshift and premature stop codon.

The gRNA sequence and genotyping primers used were:

gRNA binding site: 5'-GATGGTGACTAAGACGCGA-3'
Forward genotyping primer: 5'-CTTCCTTAGATCCTGACGTGTG-3'
Reverse genotyping primer: 5'-TATTGATGGGTTCGTCACCAG-3'

F0 *pdgfrb* crispants used were generated using Alt-R CRISPR-Cas9 reagents (IDT). The gRNA sequence and genotyping primers used were:

Dr.Cas9.PDGFRB.1.AA: 5'-GATGGTGACTAAGACGCGAG-3'
Forward genotyping primer: 5'-CTTCCTTAGATCCTGACGTGTG-3'
Reverse genotyping primer: 5'-TATTGATGGGTTCGTCACCAG-3'
Dr.Cas9.PDGFRB.1.AB: 5'-CTCGGTGCACACATAAACCC-3'
Forward genotyping primer: 5'-GACGAGAACATCCCAGACTTTC 3'
Reverse genotyping primer: 5'-GCGTGTAAACAAATCCTAACGG-3'

Throughout this study, sibling control fish were pooled homozygous wild-type and heterozygous animals, as no significant differences were detected between these genotypes (e.g. Extended Data Fig. 1c-d).

Fluorescent tracer injections

Fluorescently conjugated tracers used were: 1 kDa NHS Ester–Alexa Fluor™ 405 (Thermo Fisher: A30000), 10 kDa Dextran–Cascade Blue (Thermo Fisher: D1976), 10 kDa Dextran–Alexa Fluor™ 647 (Thermo Fisher: D22914), 70 kDa Dextran–Fluorescein (Thermo Fisher: D1822), 2000 kDa Dextran–Tetramethylrhodamine (Thermo Fisher: D7139) each at 5 mg/mL.

Larvae (3–7 dpf) were anesthetized with tricaine and embedded in 0.5% low-melting agarose (Bio-Rad 1613112) in E3 water on 35-mm glass-bottom dishes (MatTek P35G-1.5-20-C). Approximately 5 nl was injected into the posterior cardinal vein (PCV). At 14 dpf, tracers were injected into the PCV with ~10 nL tracer on 3% agarose pads. In juveniles and adults retro-orbital injections were performed[63] on 3% agarose pads, with 0.2 μL or 0.5 μL tracer respectively. Tracers were injected individually or co-injected (1–70 kDa with 2000 kDa) depending on experimental design.

Imaging

Sample preparation

For live imaging at 3-14 dpf, larvae were mounted in 0.5% low-melting point agarose in E3 embryo water on a 35-mm glass bottom dish as previously described[64]. For fixed tissue imaging, zebrafish were euthanized with tricaine overdose (10 g/L), fixed (as whole or after brain extraction) in 4% paraformaldehyde (PFA) at 4°C overnight and washed in PBS. Brains were embedded in 7% low-melting agarose in PBS (Tissue-Tek cryomolds) and coronally sectioned at 200 μm thickness using a vibrating microtome (Leica VT1000 S). Sections were mounted in RapiClear 1.52 solution (SunJin Lab, RC152201) for 3 hours at room temperature prior to imaging. Whole fish or brain samples were cleared using CUBIC clearing adapted from a previously described protocol[44]. Briefly,

samples were incubated in CUBIC-L solution at 37°C overnight after fixation, washed and incubated in PBS at 4°C overnight, then incubated in CUBIC-R solution at room temperature overnight. Samples were embedded in 2% agarose in CUBIC-R on a 35-mm glass bottom dish for imaging.

Image acquisition

Imaging was performed using the following microscopes and objectives: Olympus FV-MPERS upright multiphoton, 25x water dipping 1.05 NA (Fig. 1a-b,f; Extended Data Fig. 5e), Olympus FV3000 confocal 10x air 0.4 NA (Fig. 3a-a'; Fig. 4b-b',c',d-d'; Fig. 5a-a'; Extended Data Fig. 5f) and 40x oil immersion 1.4 NA (Fig. 5d-e), Olympus/Evident FV4000 confocal 10x air 0.4 NA (Extended Data Fig. 2d-e; Fig. 3b-b'; Extended Data Fig. 4b,d; Fig. 5b,f,g; Extended Data Fig. 6a-b'') and 30x silicone immersion 1.05 NA (Extended Data Fig. 1b; Fig. 2a,c,e; Extended Data Fig. 2b; Fig. 3c; Extended Data Fig. 4a-a'',b',c-c'; Fig. 5b') Nikon TiE with Yokogawa CSU-W1 spinning disk, Andor Sona sCMOS camera, 10x air 0.45 NA (Extended Data Fig. 5a,b), 20x air 0.75 NA (Extended Data Fig. 3c; Extended Data Fig. 5a') and 40x water immersion 1.15 NA (Extended Data Fig. 3a). For tracer leakage assays, live imaging was performed at 2 hours post-injection (hpi), with a maximum variation in timing of 15 minutes due to the sequential imaging. Fixed tissue samples were collected at 0.5 hpi (Fig. 5f, Extended Data Fig. 6), 2 hpi (Extended Data Fig. 2d–e, Fig. 4b-d', Fig. 5a–b',d–e, Extended Data Fig. 5a–b) or 6 hpi (Fig. 5g). Stereomicroscope images were acquired using an NSZ-606 Zoom Stereomicroscope with a Tucsen Photonics Co. camera using TCapture/IS Capture software.

Transmission electron microscopy

Brains were extracted from euthanized 5-month-old zebrafish, fixed in 2.5% glutaraldehyde for 1 hour at room temperature and washed in PBS. For sectioning, the brains were embedded in 7% low-melting point agarose in PBS in cryomolds (Tissue-Tek) and were sectioned coronally using a vibrating microtome (Leica VT1000 S) with 200 µm thickness. Tissue sections were processed as described previously[65]. Briefly, tissue sections were immersed consecutively in a series of aqueous solutions: 1.5% potassium ferricyanide and 2% osmium tetroxide, 1% thiocarbohydrazide, 2% osmium tetroxide, 2% uranyl acetate and 0.06% lead nitrate using a Pelco Biowave at 80W under vacuum for 3 min each. Vibratome sections then underwent serial dehydration in increasing concentrations of ethanol, before serial infiltration with increasing concentrations of Procure 812 resin. Ultrathin sections were obtained using a Leica UC64 ultramicrotome and imaged on a JEOL JEM-1011 at 80 kV.

Image processing

Images were processed using Fiji[66] or Imaris 10.1 (Bitplane). Fluorescent images are shown as maximum intensity projections (MIP), unless otherwise indicated. Vascular tracing (Fig. 1c) and masked head regions (Extended Data Fig. 1b) are presented as snapshots, and videos highlighting the hotspot leakage sites were generated using Imaris 10.1 and annotated in Adobe Premier Pro 2024. Schematics were prepared in Adobe Illustrator 2025, and pseudocolor overlays on transmission electron microscopy images were generated in Adobe Photoshop 2024.

Quantification of phenotypes

Gross anatomy

Prior to imaging and genotyping, fish body lengths were measured from the tip of the head to the tail base. Body length datasets were compiled from multiple independent experiments. Survival was quantified using separately housed *pdgfrb*^{uq30bh} mutants and siblings to enable continuous tracking. Sibling and mutant groups were initially sorted based on *pdgfrb:EGFP*-positive cells in the brain using *TgBAC(pdgfrb:EGFP)*^{uq15bh}, and were genotyped by PCR at the endpoint for each animal. Cerebrovascular aneurysms in juvenile *pdgfrb* mutants were qualitatively classified as mild or severe on the basis of aneurysm size relative to sibling controls.

Mural cell number, vessel length, diameter and branching points

Mural cell number was quantified by counting *pdgfrb:EGFP*-positive cells (*TgBAC(pdgfrb:EGFP)*^{uq15bh}) in the brain associated with blood vessels (*Tg(kdrl:Hsa.HRAS-mCherry)*^{s916}) in 3D view using Imaris 10.1. Vessel length, diameter and branching points were quantified in Imaris 10.1. At larval stages, the lumenized midbrain central arteries (*Tg(kdrl:Hsa.HRAS-mCherry)*^{s916}) branching from the middle mesencephalic central arteries (MMCtA) was traced using the Filament tool and the total filament length (μm) was plotted. Branching points within the traced vasculature were counted manually in 3D view. For adults, 100-μm thick maximum intensity projections (MIP) were generated from whole brain imaging, using the continuation of the left MMCtA as an anatomical landmark to define a consistent region of interest. For diameter measurements, 10 capillary diameters were measured per sample. Vessel anatomy was assigned using Isogai et al[67] as reference.

Tracer intensity

The quantification of tracer intensity was performed on genotype blinded image sets using Imaris 10.1 (Bitplane) and Fiji[66] in 50-μm thick MIPs, generated starting from 50 μm below the dorsal longitudinal vessel (DLV) to avoid including potential leakage from surface vessels. For live imaging quantifications, two different methods were used to validating findings. In the first method, the midbrain region was masked using the tracer accumulation in the skin as an outer boundary and metencephalic vessels as the border with the hindbrain. Vasculature was then masked and removed using *Tg(kdrl:EGFP)*^{s843} *or Tg(kdrl:Hsa.HRAS-mCherry)*^{s916}, and mean intensity of extravasated tracer within the midbrain was measured. Relative leakage by molecular weight in wild-type animals was assessed by normalizing extravasated midbrain tracer intensity to intravascular tracer intensity. For comparisons between groups (siblings versus *pdgfrb* mutants, or for wild-type at 3 versus 7 dpf), extravasated midbrain tracer intensity was normalized to vascular reporter intensity (*kdrl:EGFP* or *kdrl:Hsa.HRAS-mCherry*). In the second method, in experiments including 2000-kDa dextran as an injection control, extravasated 70- or 10-kDa dextran intensity in midbrain parenchyma was calculated from the average intensity in four defined parenchymal regions. These values were normalized to the vascular intensity of 2000-kDa dextran, calculated from the average intensity in four regions within the DLV lumen. As such, for each data point: intensity=parenchymal tracer (10 or 70 kDa) intensity/luminal 2000-kDa tracer intensity. For datasets assessing leakage between siblings versus *pdgfrb* mutants at 7 and 14 dpf (Fig. 2, Extended Data Fig. 3), we assessed the raw (non-normalized) tracer intensity in the parenchyma and compared these values to normalized values. We found that both normalization strategies improved the analysis, reducing variance and controlling for differences in tracer delivery and image variation between animals.

For tracer intensity quantification in sectioned brains, 50-μm thick MIPs were generated. Tracer intensity outside the vasculature was measured at ~70-μm intervals from medial to lateral within a 0.7-mm region in juveniles, and at ~100-μm intervals within a 1-mm region in adults, due to differences in brain size. For tracer intensity quantification in sectioned brains, 50-μm thick MIPs were generated and dextran intensity outside the vessels was measured at approximately every 70 μm from medial to lateral direction within 0.7 mm in juveniles and at every 100 μm within 1 mm in adults due to size difference. These measurements were normalized to vascular reporter intensity (*kdrl:EGFP*). MMCtAs served as anatomical landmarks to ensure consistent region selection.

Hotspot leakage sites

Hotspot leakage sites were identified as prominent focal accumulations of fluorescent tracer adjacent to and outside the vasculature. Quantification was performed in 3D using Imaris 10.1.

TEM quantification

Imaged sections were quantified using Fiji[66]. Caveolae were defined as circular profiles of less than 100 nm in diameter and were scored as luminal or abluminal based on proximity to each surface membrane (within 500 nm of each surface or in a thin-walled vessel the caveolae closest to

each surface). Basement membrane thickness was scored in six different locations per vessel that were selected at random.

Statistical analysis

Graphic representations and statistical analyses were performed using GraphPad Prism 10. Shapiro–Wilk test was applied to test normal distribution of the data. Two-tailed Student's t-tests were used for two-group comparisons with normal distribution, and Mann–Whitney U tests for non-normal data. One- or two-way ANOVA followed by Tukey's post hoc test was used for multiple group comparisons. $P<0.05$ was considered statistically significant.

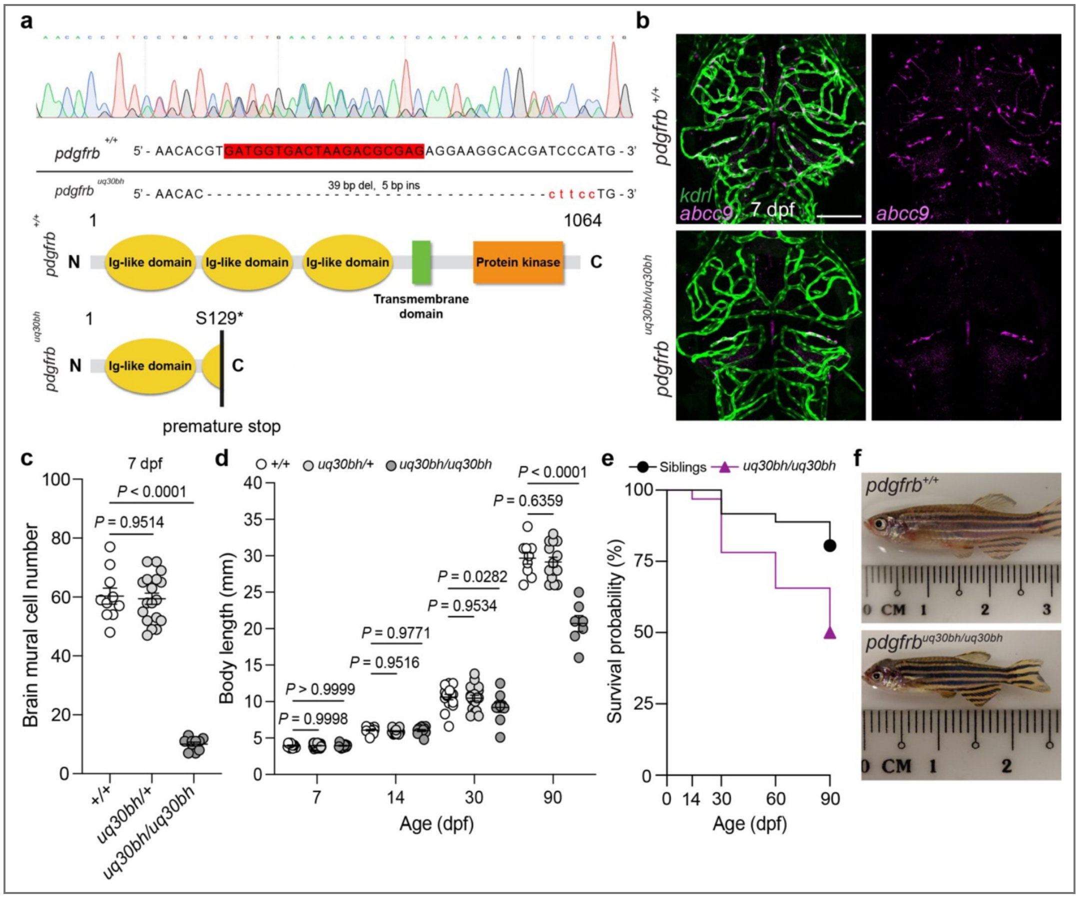

Extended Data Fig. 1. ***uq30bh* is a predicted null allele of *pdgfrb* causing brain pericyte deficiency. a**, Schematic of the CRISPR/Cas9-mediated mutation in the *pdgfrb* gene. The *uq30bh* allele carries a 39-bp deletion and a 5-bp insertion, resulting in a premature stop codon in the *pdgfrb* coding sequence, and is predicted to be a null allele. **b**, Confocal projections of pericytes (*TgBAC(abcc9:abcc9-T2A-mCherry)^{um139}*) and brain vasculature (*Tg(kdrl:Hsa.HRAS-mCherry)^{s916}*) in wild-type siblings and *pdgfrb^{uq30bh}* mutants at 7 dpf. Dorsal view, anterior up, scale bar: 100 μm. **c**, Quantification of brain mural cell numbers using the data shown in Fig. 1a. *pdgfrb:EGFP*-positive cells associated with central arteries were counted. Data are mean±SEM, n=10 *pdgfrb$^{+/+}$*, 18 *pdgfrb$^{uq30bh/+}$*, 10 *pdgfrb$^{uq30bh/uq30bh}$*, one-way ANOVA followed by multiple comparisons with Tukey's correction. **d**, Body lengths measurements of developing *pdgfrb* mutants and siblings from tip of the head to tail base at larval to adult stages. Data are mean±SEM, n=13–17 *pdgfrb$^{+/+}$*, 14–20 *pdgfrb$^{uq30bh/+}$*, 7–14 *pdgfrb$^{uq30bh/uq30bh}$* per timepoint, two-way ANOVA followed by multiple comparisons with Tukey's correction. **e**, Kaplan–Meier survival curves of siblings (n=35) and *pdgfrb^{uq30bh}* mutants (n=33), selected based on presence or absence of brain pericytes, using *TgBAC(pdgfrb:EGFP)^{uq15bh}*. Log-rank (Mantel–Cox) test, p=0.0070. **f**, Gross anatomy of adult wild-type siblings and *pdgfrb^{uq30bh}* mutants at 90 dpf. *pdgfrb^{uq30bh}* mutants exhibit reduced overall body size and craniofacial defects consistent with previously described null mutant alleles.

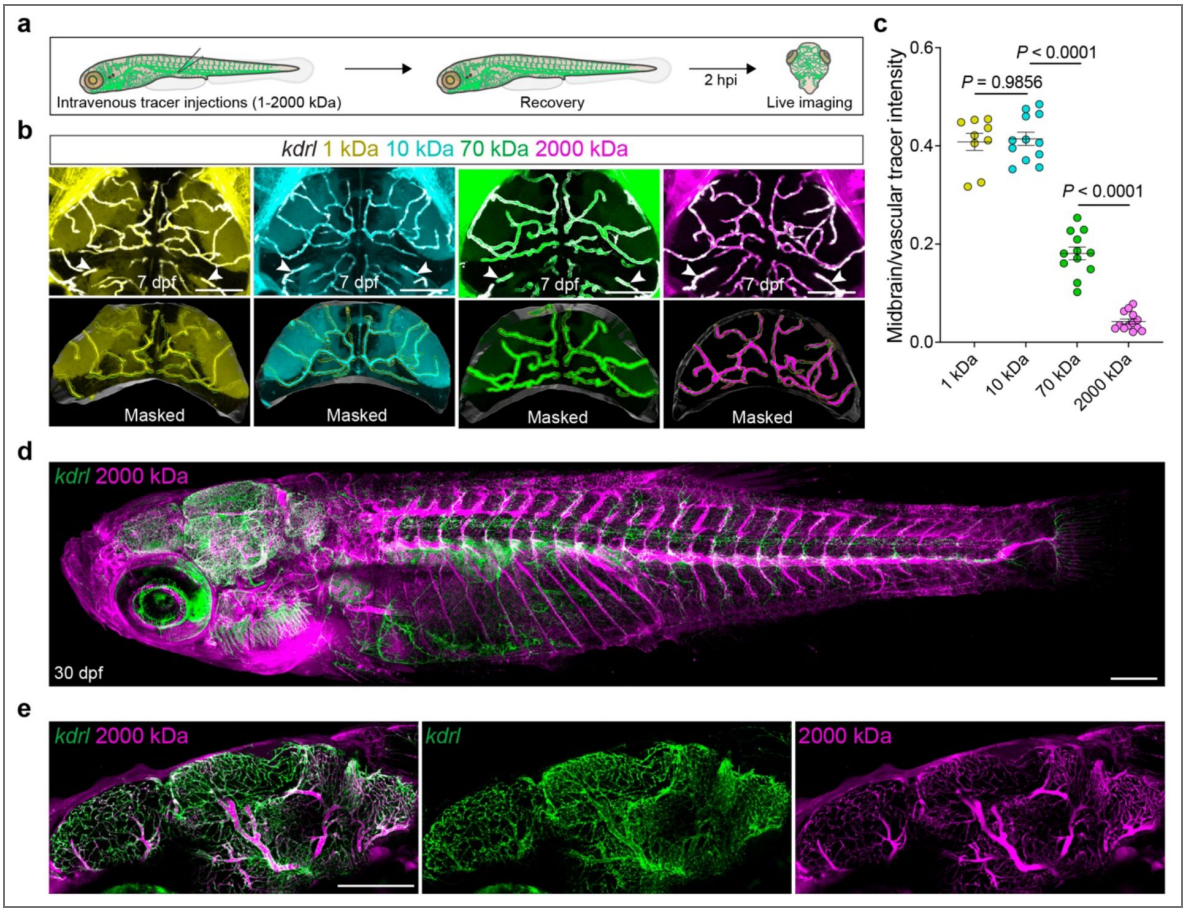

Extended Data Fig. 2. Controls for size-dependent tracer extravasation and distribution at larval and adult stages.

a, Schematic of fluorescent tracer leakage assay workflow in larvae. Tracers (1–2000 kDa) were intravenously injected, and fish were live imaged at ~2 hpi. **b**, Confocal projections of tracer leakage assays in midbrain at 7 dpf, showing negative correlation between extravasation and tracer molecular weight. Larvae were imaged with *kdrl* reporter (gray) and intravenously injected 1 kDa NHS Ester–Alexa Fluor™ 405, 10 kDa Dextran–Alexa Fluor™ 647, 70 kDa Dextran–Fluorescein, or 2000 kDa Dextran–Tetramethylrhodamine. Masked regions show the quantified region in the midbrain. The vasculature was masked (yellow) with *Tg(kdrl:EGFP)*^{s843} in the 1-, 10- and 2000-kDa tracer injections and with *Tg(kdrl:Hsa.HRAS-mCherry)*^{s916} in the 70-kDa tracer injection. The midbrain was masked (gray) using the tracer accumulation in the skin for outer lining and using the metencephalic vessels (arrowheads) for posterior border. Dorsal views, anterior up, scale bars: 100 µm. **c**, Quantification of midbrain parenchymal tracer fluorescence intensity normalized to vascular tracer fluorescence intensity. Data are mean±SEM, n=9 for 1 kDa, 12 for 10 kDa and 70 kDa, 13 for 2000 kDa, one-way ANOVA followed by multiple comparisons with Tukey's correction, $p<0.0001$ for all undisplayed pairwise comparisons. **d**–**e**, Confocal projections of cleared juvenile zebrafish at 30 dpf showing retro-orbitally injected 2000 kDa Dextran–Tetramethylrhodamine diffusing across the vasculature. (**e**) shows a subset of z-slices from (**d**) focused on the mid-sagittal region of the brain, highlighting tracer distribution throughout the brain vasculature. Lateral view, anterior to left, scale bars: 500 µm.

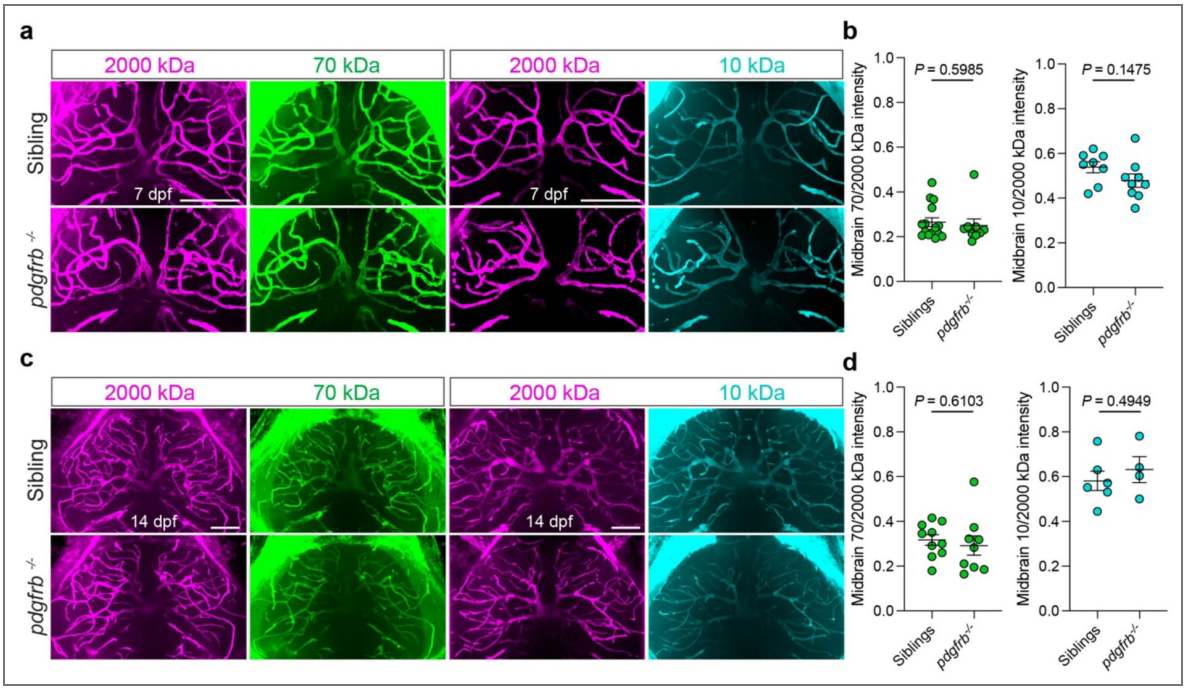

Extended Data Fig. 3. Tracer assays using an independent normalization method confirm that BBB integrity is maintained in *pdgfrb* mutant larvae.

a, **c**, Tracer leakage assays in the midbrain of zebrafish larvae in siblings and *pdgfrb* mutants at 7 dpf (**a**) and 14 dpf (**c**). 70 kDa Dextran–Fluorescein or 10 kDa Dextran–Cascade Blue was co-injected with 2000 kDa Dextran–Tetramethylrhodamine to detect parenchymal extravasation and injection volume. Dorsal views, anterior up, scale bars: 100 µm. **b**, **d**, Quantification of midbrain parenchymal 70- and 10-kDa dextran fluorescence intensity normalized to vascular 2000-kDa dextran fluorescence intensity. Data are mean±SEM. At 7 dpf (**b**): n=15 siblings and 9 *pdgfrb*$^{-/-}$ for 70 kDa, and n=8 siblings and 9 *pdgfrb*$^{-/-}$ for 10 kDa. At 14 dpf (**d**): n=10 siblings and 9 *pdgfrb*$^{-/-}$ for 70 kDa, and n=6 siblings and 4 *pdgfrb*$^{-/-}$ for 10 kDa. Unpaired t-tests for 10 kDa at 7 and 14 dpf, 70 kDa at 14 dpf. Mann–Whitney U test for 70 kDa at 7 dpf due to non-normal distribution.

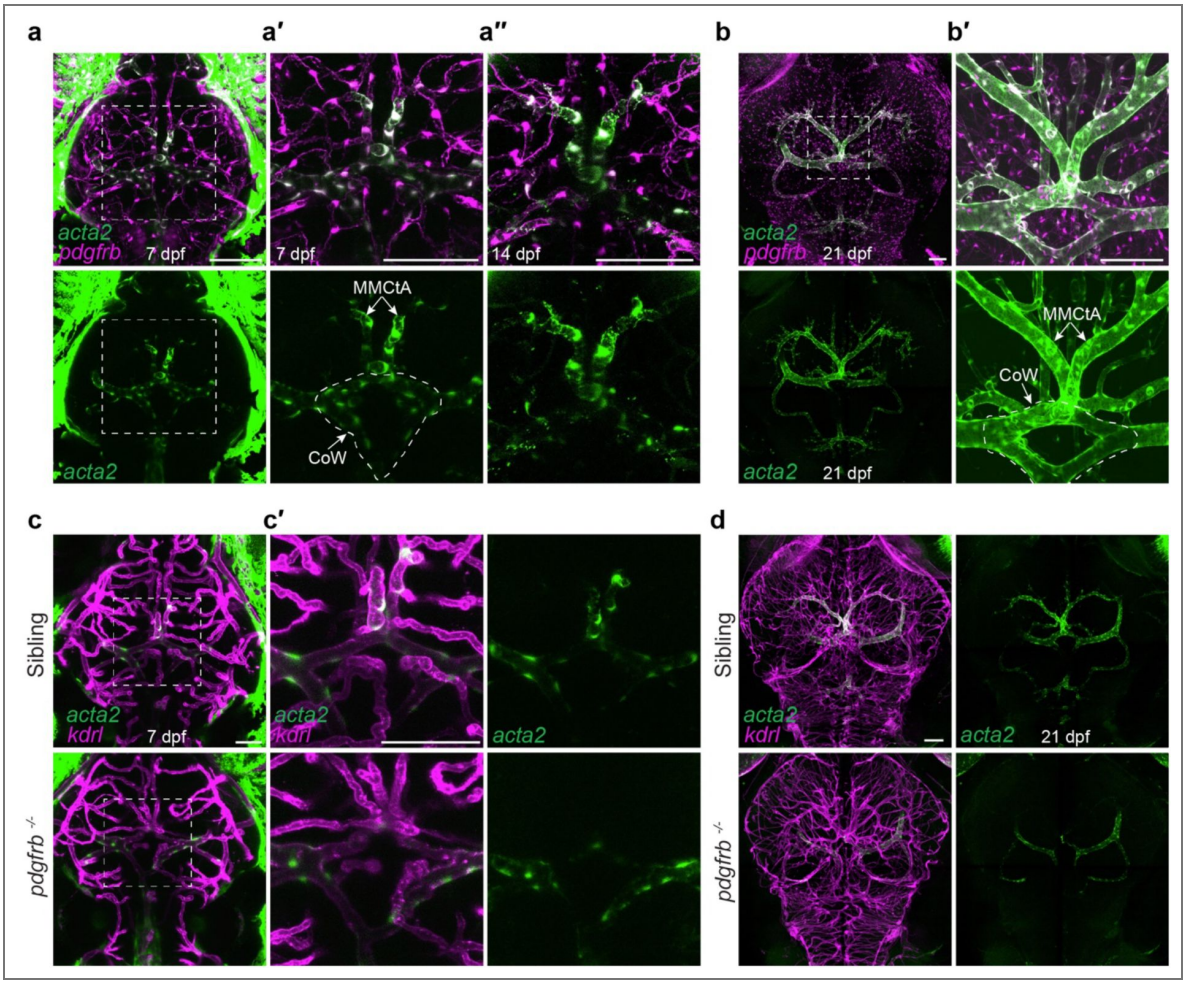

Extended Data Fig. 4. Development of *acta2:EGFP*-positive vSMCs in brain vasculature of siblings and *pdgfrb* mutants.

a–b', Confocal projections of mural cells using *TgBAC(pdgfrb:gal4FF)*^{um140}; *Tg(5xUAS:RFP)*^{nkuasrfp1a} and *TgBAC(acta2:EGFP)*^{uq17bh}, live imaged at 7 and 14 dpf (**a–a'**) or imaged at 21 dpf post-fixation and clearing (**b–b'**).*acta2:EGFP* colocalizes with *RFP* driven by *pdgfrb:gal4FF* along MMCtAs (arrows) and at the Circle of Willis (CoW) (dashed line) by 7 dpf, expanding to arterioles by 21 dpf but absent from capillaries. (**a'**) and (**b'**) are enlarged views of white boxes in (**a**) and (**b**), respectively. (**a''**) shows the same fish reimaged at 14 dpf. **c–d'**, Confocal projections of developing smooth muscle cells (*TgBAC(acta2:EGFP)*^{uq17bh}) and brain vasculature (*Tg(kdrl:Hsa.HRAS-mCherry)*^{s916}) in siblings and *pdgfrb* mutants live imaged at 7 dpf (**c–c'**) or imaged at 21 dpf post-fixation and clearing (**d**). White boxes are magnified in (**c'**). **a–d**, Dorsal views, anterior up, scale bars: 100 μm (**a–b'**, **d**), 50 μm (**c–c'**).

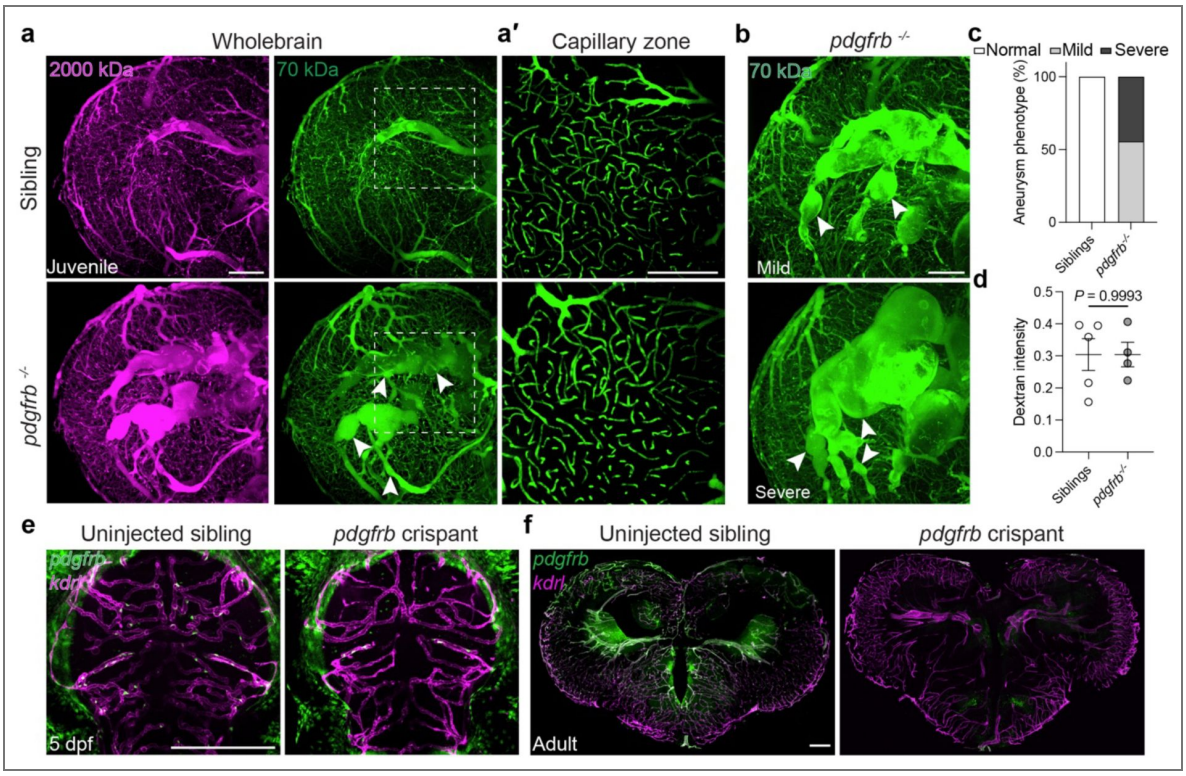

Extended Data Fig. 5. Arterial aneurysms in juvenile *pdgfrb* mutants and additional control data.

a, Fluorescent tracer leakage assays in 2-month-old zebrafish midbrain (2 hpi). 70 kDa Dextran–Fluorescein and 2000 kDa Dextran–Tetramethylrhodamine were co-injected to detect parenchymal extravasation and vascular tracer, respectively. Arrowheads mark aneurysms. **a'**, Same brains reimaged at higher resolution targeting capillary regions. 30-µm-thick MIPs were displayed, starting 30 µm below the most superficial point of left hemisphere to exclude potential leakage from meningeal vessels. **b**, Examples of mild and severe aneurysms (arrowheads) in *pdgfrb* mutants. **c**, Quantification of the severity of aneurysms in sibling and *pdgfrb* mutants. Aneurysm phenotypes were qualitatively categorised based on severity; normal, mild and severe, n=11 per group. **d**, Quantification of parenchymal 70-kDa Dextran intensity normalized to vascular 2000 kDa Dextran intensity using the data in (**a'**). Data are mean±SEM, n=5 sibling and 4 *pdgfrb*$^{-/-}$, unpaired t-test. **e–f**, Validation that crispants phenocopy *pdgfrb* mutants (supporting data in Fig. 5d–e). Maximum intensity projections of mural cells (*TgBAC(pdgfrb:EGFP)*^{uq15bh}) and brain vasculature (*Tg(kdrl:Hsa.HRAS-mCherry)*^{s916}) in uninjected sibling and *pdgfrb* crispants at larva (5 dpf) and adult (10-week-old) stage. *pdgfrb* crispants lack brain mural cells and show dilated arteries in adulthood, phenocopying *pdgfrb*^{uq30bh} mutants. **a–b**, **e**, Dorsal views, anterior up. **a–b**, **e–f**, Scale bars: 200 µm.

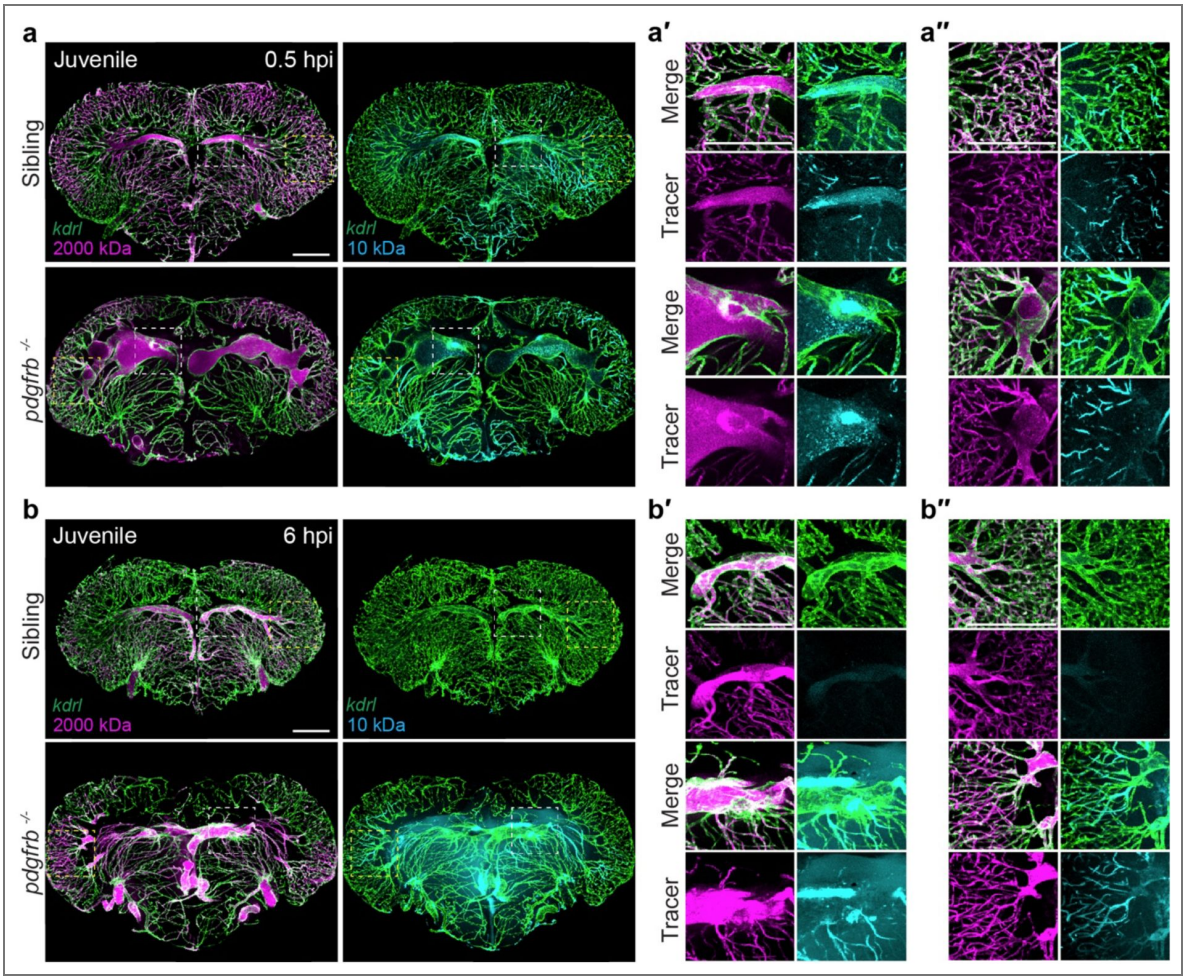

Extended Data Fig. 6. Coronal midbrain sections corresponding to Fig. 5f-g.

a, **b**, Entire coronal midbrain sections from tracer leakage assays in 1-month-old sibling and *pdgfrb* mutants shown as confocal projections. Brains were collected after retro-orbital co-injection of 10 kDa Dextran–Alexa Fluor™ 647 and 2000 kDa Dextran–Tetramethylrhodamine at 0.5 hpi (**a**) or 6 hpi (**b**), and *Tg(kdrl:EGFP)*^{s843} was used to label vasculature. **a'–a''**, **b'–b''**, Enlarged views of regions indicated in (**a**) and (**b**). Panels (**a'**) and (**b'**) show medial regions (white boxes), whereas (**a''**) and (**b''**) show lateral regions (yellow boxes) in midbrain. Perfusion of tracer dyes and leakage hotspots are readily identifiable. Scale bars: 200 μm.

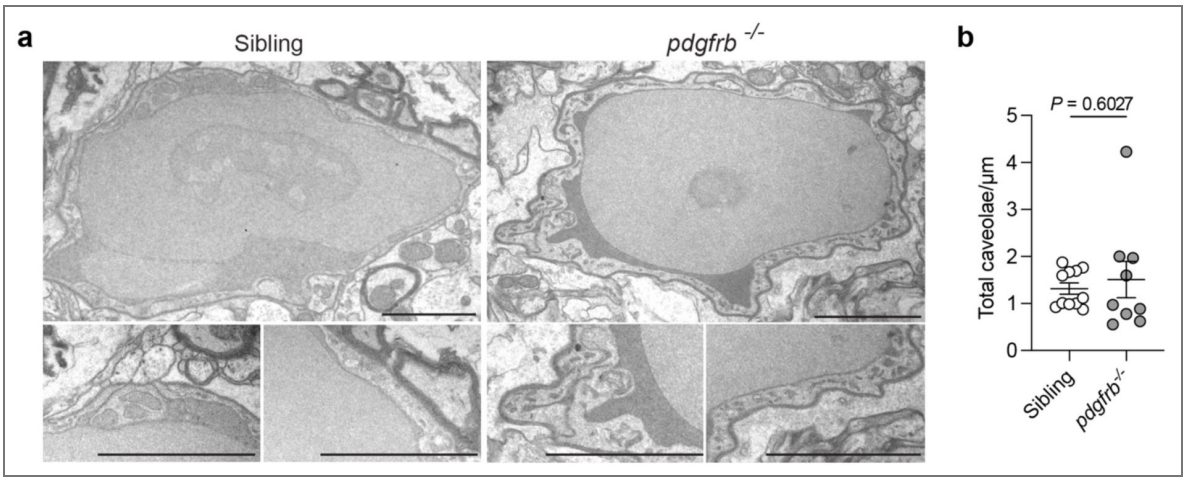

Extended Data Fig. 7. Adult *pdgfrb* mutants maintain normal endothelial ultrastructure in capillaries.

a, Transmission electron microscopy images of sectioned adult zebrafish brain vessels. **b**, Quantification of endothelial caveolae in capillaries of siblings and *pdgfrb* mutants. Measurements were made for n=11 vessels in siblings and 9 in *pdgfrb* mutants across n=3 animals per group. Data are mean±SEM and are not distributed normally, Mann–Whitney U test was applied. No consistent defects were observed in capillaries. Scale bars: 1 µm.

Data availability

Source datasheet 1 contains the numerical data used to generate the figures.

Acknowledgements

This project was supported in part by funding from Bright focus (A2018807S), the Australian Research Council (ARC) (DP210102712) and The Brain Cancer Centre (founded by Carrie's Beanies for Brain Cancer). B.M.H was supported by a National Health and Medical Research Council Senior Research Fellowship (1155221) and Investigator grant (2033008). R.G.P was supported by an ARC Laureate Fellowship (FL210100107). We thank the Centre for Advanced Histology and Microscopy (*RRID:SCR_025432*) at the Peter MacCallum Cancer Centre and Microscopy Australia Research Facility at the Centre for Microscopy and Microanalysis at The University of Queensland. We thank Koji Ando and Nathan Lawson for providing constructs and protocols for BAC recombineering. We also thank Kelly Smith and Marcos Sande Melon for academic discussions and technical suggestions.

Additional information

Author contributions

O.F.B performed, analyzed experiments and co-wrote manuscript. B.M.H, conceptualized experiments, analyzed data and co-wrote manuscript. A.U.G, S.D, W.W, S.P, M.C.R.G, Y.W.L, J.R, R.P, A.L and A.F performed and analyzed experiments.

Funding

Funder	Grant reference number	Author
Department of Education and Training | Australian Research Council (ARC)	DP210102712	Benjamin M Hogan
DHAC | National Health and Medical Research Council (NHMRC)	1155221	Benjamin M Hogan
DHAC | National Health and Medical Research Council (NHMRC)	2033008	Benjamin M Hogan
Department of Education and Training | Australian Research Council (ARC)	FL210100107	Robert G Parton

Author ORCID iDs

Ye-Wheen Lim: https://orcid.org/0000-0001-5878-8708
Anne Lagendijk: https://orcid.org/0000-0003-1246-1608
Robert G Parton: https://orcid.org/0000-0002-7494-5248
Benjamin M Hogan: https://orcid.org/0000-0002-0651-7065

Additional files

Source datasheet 1 Numerical data used to generate all plots presented in the figures. Source data in an excel spreadsheet in which each separate tab provides the individual measurements and numbers used to generate the plots presented in each figure.

Supplementary Video 1

Supplementary Video 2

References

1 **Zhao Z.,** Nelson A. R., Betsholtz C., Zlokovic B. V (2015) Establishment and Dysfunction of the Blood-Brain Barrier. *Cell* **163**:1064-1078 https://doi.org/10.1016/j.cell.2015.10.067 | PubMed

2 **Armulik A.,** Genove G., Betsholtz C (2011) Pericytes: developmental, physiological, and pathological perspectives, problems, and promises. *Dev Cell* **21**:193-215 https://doi.org/10.1016/j.devcel.2011.07.001 | PubMed

3 **Leveen P.,** et al. (1994) Mice deficient for PDGF B show renal, cardiovascular, and hematological abnormalities. *Genes Dev* **8**:1875-1887 https://doi.org/10.1101/gad.8.16.1875 | PubMed

4 **Lindahl P.,** Johansson B. R., Leveen P., Betsholtz C (1997) Pericyte loss and microaneurysm formation in PDGF-B-deficient mice. *Science* **277**:242-245 https://doi.org/10.1126/science.277.5323.242 | PubMed

5 **Armulik A.,** et al. (2010) Pericytes regulate the blood-brain barrier. *Nature* **468**:557-561 https://doi.org/10.1038/nature09522 | PubMed

6 **Daneman R.,** Zhou L., Kebede A. A., Barres B. A (2010) Pericytes are required for blood-brain barrier integrity during embryogenesis. *Nature* **468**:562-566 https://doi.org/10.1038/nature09513 | PubMed

7 **Eilken H. M.,** et al. (2017) Pericytes regulate VEGF-induced endothelial sprouting through VEGFR1. *Nat Commun* **8**:1574 https://doi.org/10.1038/s41467-017-01738-3 | PubMed

8 **Simonavicius N.,** et al. (2012) Pericytes promote selective vessel regression to regulate vascular patterning. *Blood* **120**:1516-1527 https://doi.org/10.1182/blood-2011-01-332338 | PubMed

9 **Benjamin L. E.,** Hemo I., Keshet E (1998) A plasticity window for blood vessel remodelling is defined by pericyte coverage of the preformed endothelial network and is regulated by PDGF-B and VEGF. *Development* **125**:1591-1598 https://doi.org/10.1242/dev.125.9.1591 | PubMed

10 **Hellstrom M.,** Kalen M., Lindahl P., Abramsson A., Betsholtz C (1999) Role of PDGF-B and PDGFR-beta in recruitment of vascular smooth muscle cells and pericytes during embryonic blood vessel formation in the mouse. *Development* **126**:3047-3055 https://doi.org/10.1242/dev.126.14.3047 | PubMed

11 **Hirschi K. K.,** Rohovsky S. A., D'Amore P. A. (1998) PDGF, TGF-beta, and heterotypic cell-cell interactions mediate endothelial cell-induced recruitment of 10T1/2 cells and their differentiation to a smooth muscle fate. *J Cell Biol* **141**:805-814 https://doi.org/10.1083/jcb.141.3.805 | PubMed

12 **Soriano P** (1994) Abnormal kidney development and hematological disorders in PDGF beta-receptor mutant mice. *Genes Dev* **8**:1888-1896 https://doi.org/10.1101/gad.8.16.1888 | PubMed

13 **Ando K.,** et al. (2021) Conserved and context-dependent roles for pdgfrb signaling during zebrafish vascular mural cell development. *Dev Biol* **479**:11-22 https://doi.org/10.1016/j.ydbio.2021.06.010 | PubMed

14 **Mae M. A.,** et al. (2021) Single-Cell Analysis of Blood-Brain Barrier Response to Pericyte Loss. *Circ Res* **128**:e46-e62 https://doi.org/10.1161/CIRCRESAHA.120.317473 | PubMed

15 **Paredes-Gonzalez S.,** Salazar-Tirado J., Recabal-Beyer A., Contreras E. G (2025) Invertebrate glial barriers as a model for understanding blood-brain barrier evolution. *Fluids Barriers CNS* **22** https://doi.org/10.1186/s12987-025-00694-1 | PubMed

16 **Limmer S.,** Weiler A., Volkenhoff A., Babatz F., Klambt C (2014) The Drosophila blood-brain barrier: development and function of a glial endothelium. *Front Neurosci* **8** https://doi.org/10.3389/fnins.2014.00365 | PubMed

17 **Jeong J. Y.,** et al. (2008) Functional and developmental analysis of the blood-brain barrier in zebrafish. *Brain Res Bull* **75**:619-628 https://doi.org/10.1016/j.brainresbull.2007.10.043 | PubMed

18 **Xie J.,** Farage E., Sugimoto M., Anand-Apte B (2010) A novel transgenic zebrafish model for blood-brain and blood-retinal barrier development. *BMC Dev Biol* **10** https://doi.org/10.1186/1471-213X-10-76 | PubMed

19 **Quinonez-Silvero C.,** Hubner K., Herzog W (2020) Development of the brain vasculature and the blood-brain barrier in zebrafish. *Dev Biol* **457**:181-190 https://doi.org/10.1016/j.ydbio.2019.03.005 | PubMed

20 **Umans R. A.,** et al. (2017) CNS angiogenesis and barriergenesis occur simultaneously. *Dev Biol* **425**:101-108 https://doi.org/10.1016/j.ydbio.2017.03.017 | PubMed

21 **O'Brown N. M.,** Megason S. G., Gu C (2019) Suppression of transcytosis regulates zebrafish blood-brain barrier function. *eLife* **8** https://doi.org/10.7554/eLife.47326 | PubMed

22 **Li Y.,** et al. (2022) Claudin-5a is essential for the functional formation of both zebrafish blood-brain barrier and blood-cerebrospinal fluid barrier. *Fluids Barriers CNS* **19** https://doi.org/10.1186/s12987-022-00337-9 | PubMed

23 **Vanhollebeke B.,** et al. (2015) Tip cell-specific requirement for an atypical Gpr124- and Reck-dependent Wnt/beta-catenin pathway during brain angiogenesis. *eLife* **4** https://doi.org/10.7554/eLife.06489 | PubMed

24 **Guemez-Gamboa A.,** et al. (2015) Inactivating mutations in MFSD2A, required for omega-3 fatty acid transport in brain, cause a lethal microcephaly syndrome. *Nat Genet* **47**:809-813 https://doi.org/10.1038/ng.3311 | PubMed

25 **Ben-Zvi A.,** et al. (2014) Mfsd2a is critical for the formation and function of the blood-brain barrier. *Nature* **509**:507-511 https://doi.org/10.1038/nature13324 | PubMed

26 **Andreone B. J.,** et al. (2017) Blood-Brain Barrier Permeability Is Regulated by Lipid Transport-Dependent Suppression of Caveolae-Mediated Transcytosis. *Neuron* **94**:581-594 e585 https://doi.org/10.1016/j.neuron.2017.03.043 | PubMed

27 **Eubelen M.,** et al. (2018) A molecular mechanism for Wnt ligand-specific signaling. *Science* **361** https://doi.org/10.1126/science.aat1178 | PubMed

28 **Parab S.,** et al. (2023) Local angiogenic interplay of Vegfc/d and Vegfa controls brain region-specific emergence of fenestrated capillaries. *eLife* **12** https://doi.org/10.7554/eLife.86066 | PubMed

29 **Parab S.,** Quick R. E., Matsuoka R. L (2021) Endothelial cell-type-specific molecular requirements for angiogenesis drive fenestrated vessel development in the brain. *eLife* **10** https://doi.org/10.7554/eLife.64295 | PubMed

30 **Shih Y. H.,** Portman D., Idrizi F., Grosse A., Lawson N. D (2021) Integrated molecular analysis identifies a conserved pericyte gene signature in zebrafish. *Development* **148** https://doi.org/10.1242/dev.200189 | PubMed

31 **Ando K.,** et al. (2016) Clarification of mural cell coverage of vascular endothelial cells by live imaging of zebrafish. *Development* **143**:1328-1339 https://doi.org/10.1242/dev.132654 | PubMed

32 **Ulrich F.,** et al. (2016) Reck enables cerebrovascular development by promoting canonical Wnt signaling. *Development* **143**:1055 https://doi.org/10.1242/dev.136507 | PubMed

33 **Wang Y.,** Pan L., Moens C. B., Appel B (2014) Notch3 establishes brain vascular integrity by regulating pericyte number. *Development* **141**:307-317 https://doi.org/10.1242/dev.096107 | PubMed

34 **Ando K.,** et al. (2019) Peri-arterial specification of vascular mural cells from naive mesenchyme requires Notch signaling. *Development* **146** https://doi.org/10.1242/dev.165589 | PubMed

35 **Ando K.,** Ishii T., Fukuhara S (2021) Zebrafish Vascular Mural Cell Biology: Recent Advances, Development, and Functions. *Life* **11** https://doi.org/10.3390/life11101041 | PubMed

36 **Gall L. G.,** et al. (2025) Zebrafish glial-vascular interactions progressively expand over the course of brain development. *iScience* **28** https://doi.org/10.1016/j.isci.2024.111549 | PubMed

37 **Chen J.,** Poskanzer K. E., Freeman M. R., Monk K. R (2020) Live-imaging of astrocyte morphogenesis and function in zebrafish neural circuits. *Nat Neurosci* **23**:1297-1306 https://doi.org/10.1038/s41593-020-0703-x | PubMed

38 **Mayer M. G.,** Fischer T (2024) Microglia at the blood brain barrier in health and disease. *Front Cell Neurosci* **18**:1360195 https://doi.org/10.3389/fncel.2024.1360195 | PubMed

39 **Wu S.,** et al. (2018) Il34-Csf1r Pathway Regulates the Migration and Colonization of Microglial Precursors. *Dev Cell* **46**:552-563 e554 https://doi.org/10.1016/j.devcel.2018.08.005 | PubMed

40 **Xu J.,** et al. (2015) Temporal-Spatial Resolution Fate Mapping Reveals Distinct Origins for Embryonic and Adult Microglia in Zebrafish. *Dev Cell* **34**:632-641 https://doi.org/10.1016/j.devcel.2015.08.018 | PubMed

41 **Herbomel P.,** Thisse B., Thisse C (2001) Zebrafish early macrophages colonize cephalic mesenchyme and developing brain, retina, and epidermis through a M-CSF receptor-dependent invasive process. *Dev Biol* **238**:274-288 https://doi.org/10.1006/dbio.2001.0393 | PubMed

42 **Gaudi A. U.,** et al. (2026) Convergent evolution of scavenger cell development at brain borders. *Nature* https://doi.org/10.1038/s41586-025-10003-3 | PubMed

43 **Lim Y. W.,** et al. (2026) Trans-Endothelial Trafficking in Zebrafish: Nanobio Interactions of Polyethylene Glycol-Based Nanoparticles in Live Vasculature. *ACS Nano* https://doi.org/10.1021/acsnano.5c21042 | PubMed

44 **Matsumoto K.,** et al. (2019) Advanced CUBIC tissue clearing for whole-organ cell profiling. *Nat Protoc* **14**:3506-3537 https://doi.org/10.1038/s41596-019-0240-9 | PubMed

45 **Sinha B.,** et al. (2011) Cells respond to mechanical stress by rapid disassembly of caveolae. *Cell* **144**:402-413 https://doi.org/10.1016/j.cell.2010.12.031 | PubMed

46 **Del Pozo M. A.,** Lolo F. N., Echarri A (2021) Caveolae: Mechanosensing and mechanotransduction devices linking membrane trafficking to mechanoadaptation. *Curr Opin Cell Biol* **68**:113-123 https://doi.org/10.1016/j.ceb.2020.10.008 | PubMed

47 **Rajan A. M.,** Ma R. C., Kocha K. M., Zhang D. J., Huang P (2020) Dual function of perivascular fibroblasts in vascular stabilization in zebrafish. *PLoS Genet* **16**:e1008800 https://doi.org/10.1371/journal.pgen.1008800 | PubMed

48 **Tjakra M.,** et al. (2019) Overview of Crosstalk Between Multiple Factor of Transcytosis in Blood Brain Barrier. *Front Neurosci* **13**:1436 https://doi.org/10.3389/fnins.2019.01436 | PubMed

49 **Boye K.,** et al. (2022) Endothelial Unc5B controls blood-brain barrier integrity. *Nat Commun* **13**:1169 https://doi.org/10.1038/s41467-022-28785-9 | PubMed

50 **Ayloo S.,** et al. (2022) Pericyte-to-endothelial cell signaling via vitronectin-integrin regulates blood-CNS barrier. *Neuron* **110**:1641-1655 e1646 https://doi.org/10.1016/j.neuron.2022.02.017 | PubMed

51 **Berthiaume A. A.,** et al. (2022) Pericyte remodeling is deficient in the aged brain and contributes to impaired capillary flow and structure. *Nat Commun* **13**:5912 https://doi.org/10.1038/s41467-022-33464-w | PubMed

52 **Park D. Y.,** et al. (2017) Plastic roles of pericytes in the blood-retinal barrier. *Nat Commun* **8**:15296 https://doi.org/10.1038/ncomms15296 | PubMed

53 **Renshaw S. A.,** Trede N. S (2012) A model 450 million years in the making: zebrafish and vertebrate immunity. *Dis Model Mech* **5**:38-47 https://doi.org/10.1242/dmm.007138 | PubMed

54 **Vanlandewijck M.,** et al. (2018) A molecular atlas of cell types and zonation in the brain vasculature. *Nature* **554**:475-480 https://doi.org/10.1038/nature25739 | PubMed

55 **Bower N. I.,** et al. (2017) Mural lymphatic endothelial cells regulate meningeal angiogenesis in the zebrafish. *Nat Neurosci* **20**:774-783 https://doi.org/10.1038/nn.4558 | PubMed

56 **Hogan B. M.,** et al. (2009) Ccbe1 is required for embryonic lymphangiogenesis and venous sprouting. *Nat Genet* **41**:396-398 https://doi.org/10.1038/ng.321 | PubMed

57 **Jin S. W.,** Beis D., Mitchell T., Chen J. N., Stainier D. Y (2005) Cellular and molecular analyses of vascular tube and lumen formation in zebrafish. *Development* **132**:5199-5209 https://doi.org/10.1242/dev.02087 | PubMed

58 **Traver D.,** et al. (2003) Transplantation and in vivo imaging of multilineage engraftment in zebrafish bloodless mutants. *Nat Immunol* **4**:1238-1246 https://doi.org/10.1038/ni1007 | PubMed

59 **Asakawa K.,** et al. (2008) Genetic dissection of neural circuits by Tol2 transposon-mediated Gal4 gene and enhancer trapping in zebrafish. *Proc Natl Acad Sci U S A* **105**:1255-1260 https://doi.org/10.1073/pnas.0704963105 | PubMed

60 **Davis A. E.,** Castranova D., Weinstein B. M (2021) Rapid Generation of Pigment Free, Immobile Zebrafish Embryos and Larvae in Any Genetic Background Using CRISPR-Cas9 dgRNPs. *Zebrafish* **18**:235-242 https://doi.org/10.1089/zeb.2021.0011 | PubMed

61 **Suster M. L.,** Sumiyama K., Kawakami K (2009) Transposon-mediated BAC transgenesis in zebrafish and mice. *BMC Genomics* **10** https://doi.org/10.1186/1471-2164-10-477 | PubMed

62 **Bussmann J.,** Schulte-Merker S (2011) Rapid BAC selection for tol2-mediated transgenesis in zebrafish. *Development* **138**:4327-4332 https://doi.org/10.1242/dev.068080 | PubMed

63 **Pugach E. K.,** Li P., White R., Zon L (2009) Retro-orbital injection in adult zebrafish. *J Vis Exp* https://doi.org/10.3791/1645 | PubMed

64 **Okuda K. S.,** Baek S., Hogan B. M (2018) Visualization and Tools for Analysis of Zebrafish Lymphatic Development. *Methods Mol Biol* **1846**:55-70 https://doi.org/10.1007/978-1-4939-8712-2_4 | PubMed

65 **Lim Y. W.,** et al. (2017) Caveolae Protect Notochord Cells against Catastrophic Mechanical Failure during Development. *Curr Biol* **27**:1968-1981 e1967 https://doi.org/10.1016/j.cub.2017.05.067 | PubMed

66 **Schindelin J.,** et al. (2012) Fiji: an open-source platform for biological-image analysis. *Nat Methods* **9**:676-682 https://doi.org/10.1038/nmeth.2019 | PubMed

67 **Isogai S.,** Horiguchi M., Weinstein B. M (2001) The vascular anatomy of the developing zebrafish: an atlas of embryonic and early larval development. *Dev Biol* **230**:278-301 https://doi.org/10.1006/dbio.2000.9995 | PubMed

Peer reviews

Reviewer #1 (Public review):

Summary:

The study investigates the role of vascular mural cells, specifically pericytes and vascular smooth muscle cells (vSMCs), in maintaining blood-brain barrier (BBB) integrity and regulating vascular patterning. Analyzing zebrafish pdgfrb mutants that lack brain pericytes and vSMCs, the show that mural cell deficiency does not impair BBB establishment or maintenance during larval and early juvenile stages. However mural cells seem to be crucial for preventing vascular aneurysms and hemorrhage in adulthood as focal leakage, basement membrane disruption and increased caveolae formation are observed in adult zebrafish at aneurysm hotspots. The authors challenge the paradigm that mural cells are essential for BBB regulation in early development while highlighting their importance for long-term vascular stability.

Strengths:

Previous studies have established that the zebrafish BBB shares molecular and morphological homology with e.g. the mammalian BBB and therefore represents a suitable model. By examining mural cell roles across different life stages-from larval to adult zebrafish-the study provides an unprecedented comprehensive developmental analysis of brain vascular development and of how mural cells influence BBB integrity and vascular stability over time. The use of live imaging, whole-brain clearing, and electron microscopy offers high-resolution insights into cerebrovascular patterning, aneurysm development, and structural changes in endothelial cells and basement membranes. By analyzing "leakage hotspots" and their association with structural endothelial defects in adults the presented findings add novel insights into how mural cell loss may lead to vascular instability.

https://doi.org/10.7554/eLife.104061.2.sa2

Reviewer #2 (Public review):

Summary:

The authors generated a zebrafish mutant of the pdgfrb gene. The presented analyses and data confirm previous studies demonstrating that Pdgfrb signaling is necessary for mural cell development in zebrafish. In addition, the data support previously published studies in zebrafish showing that mural cell deficiency leads to hemorrhages later in life. The authors presented quantified data on vessel density and branching, assessed tracer extravasation, and investigated the vasculature of adult mice using electron microscopy.

Strengths:

The strength of this article is that it provides independent confirmation of the important role of Pdgfrb signaling for the development of mural cells in the zebrafish brain. In addition, it confirms previous literature on zebrafish that provides evidence that, in the absence of pericytes/VSMC, hemorrhages appear (Wang et al, 2014, PMID: 24306108 and Ando et al 2021, PMID: 3431092)".

The Reviewing Editor has carefully reviewed the revised manuscript and is fully satisfied with the authors' revisions.

https://doi.org/10.7554/eLife.104061.2.sa1

Author Response:

The following is the authors' response to the original reviews.

> ***Public Reviews:***
>
> ***Reviewer #1 (Public review):***
>
> *Summary:*
>
> *The study investigates the role of vascular mural cells, specifically pericytes and vascular smooth muscle cells (vSMCs), in maintaining blood-brain barrier (BBB) integrity and regulating vascular patterning. Analyzing zebrafish pdgfrb mutants that lack brain pericytes and vSMCs, they show that mural cell deficiency does not impair BBB establishment or maintenance during larval and early juvenile stages. However, mural cells seem to be crucial for preventing vascular aneurysms and hemorrhage in adulthood as focal leakage, basement membrane disruption, and increased caveolae formation are observed in adult zebrafish at aneurysm hotspots. The authors challenge the paradigm that mural cells are essential for BBB regulation in early development while highlighting their importance for long-term vascular stability.*
>
> *Strengths:*
>
> *Previous studies have established that the zebrafish BBB shares molecular and morphological homology with e.g. the mammalian BBB and therefore represents a suitable model. By examining mural cell roles across different life stages - from larval to adult zebrafish - the study provides an unprecedented comprehensive developmental analysis of brain vascular development and of how mural cells influence BBB integrity and vascular stability over time. The use of live imaging, whole-brain clearing, and electron microscopy offers high-resolution insights into cerebrovascular patterning, aneurysm development, and structural changes in endothelial cells and basement*

> *membranes. By analyzing "leakage hotspots" and their association with structural endothelial defects in adults the presented findings add novel insights into how mural cell loss may lead to vascular instability.*
>
> *Weaknesses:*
>
> *The study uses quantitative tracer assays with multiple molecular weight dyes to evaluate blood-brain barrier (BBB) permeability. The study normalizes the intensity of tracer signals (e.g., 10 kDa, 70 kDa dextrans) in the brain parenchyma to the vascular signal of a 2000 kDa dextran tracer (assumed to remain within vessels). Intensity normalization is used to control for variations in tracer injection efficiency or vascular density. This method doesn't directly assess the absolute amount of tracer present in the parenchyma, potentially underestimating leakage severity. As the lack of BBB impairment is a "negative" finding, more rigorous controls or other methods might be needed to corroborate it.*

In response to these and comments from other reviewers, we have now performed further carefully controlled analysis to test leakage of tracers using molecular weights ranging from 1 to 2000 kDa. We have performed additional normalisation approaches (new data in Fig. 2a–d) imaging tracer extravasation together with vascular reporters (*Tg*(*kdrl:EGFP*)^{s843} or *Tg*(*kdrl:Hsa.HRAS-mCherry*)^{s916}) and used this transgenic reporter for normalisation (as suggested by Reviewer #2). The results of these experiments all supported our initial conclusions (revised Extended Data Fig. 3a–d) further validating the reliability of our method. Furthermore, as suggested by the reviewer analysis of the raw tracer intensity amounts in the parenchyma were also performed with no normalization at all (see Author response image 1). This also supports our conclusion that the BBB is intact in young animals. Finally, we now use our methods to demonstrate that we can detect an immature leaky BBB at 3 dpf and a mature functional BBB at 7 dpf (Fig. 2e-f), a suitable positive control to show that our methods and analyses are reliable.

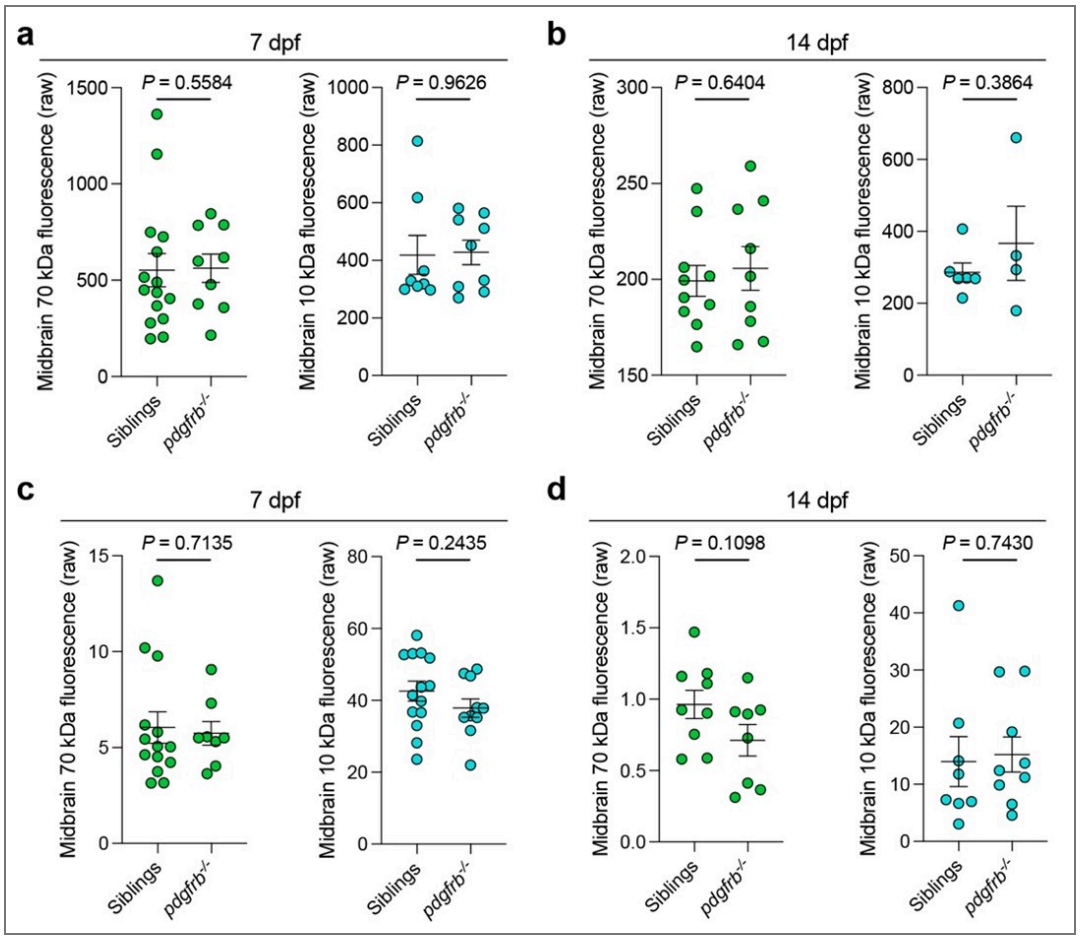

Author response image 1. Raw intensity values from the parenchyma confirm findings in Figure 2 and Extended Data Figure 3. a–d, Raw mean fluorescence intensity values of extravasated tracers in the midbrain.(a–b) show unnormalized values corresponding to Extended Data Fig. 3a–d, and (c–d) show unnormalized values corresponding to Fig. 1a–d. Unpaired t-tests for 70 and 10 kDa at 14 dpf in (a–b), for 10 kD at 7 dpf, and for 70 kDa at 14 dpf in (c–d). Mann-Whitney tests for 70 and 10 kDa at 7 dpf in (a–b), for 70 kDa at 7 dpf, and for 10 kDa at 14 dpf (c–d), due to non-normal distribution. These data were all generated in genotype blind assays, display variance in signal that is generated between embryos due to injection differences and show no difference between the genotypes analysed in BBB integrity. Comparison of this to normalised data using 2000 kDa tracer or *kdrl* expression in endothelial cells (Fig. 2 and Extended Data Fig. 3) confirms that normalisation improves the analysis, effectively controlling for embryo-to-embryo differences in delivery of tracer and imaging.

Reviewer #2 (Public review):

Summary:

The authors generated a zebrafish mutant of the pdgfrb gene. The presented analyses and data confirm previous studies demonstrating that Pdgfrb signaling is necessary for mural cell development in zebrafish. In addition, the data support previously published studies in zebrafish showing that mural cell deficiency leads to hemorrhages later in life. The authors presented quantified data on vessel density and branching, assessed tracer extravasation, and investigated the vasculature of adult mice using electron microscopy.

Strengths:

The strength of this article is that it provides independent confirmation of the important role of Pdgfrb signaling for the development of mural cells in the zebrafish brain. In addition, it confirms previous literature on zebrafish that provides evidence that, in the

> *absence of pericytes/VSMC, hemorrhages appear (Wang et al, 2014, PMID: 24306108 and Ando et al 2021, PMID: 3431092). The study by Ando et al, 2021 did not report experiments assessing BBB leakage in pdgfrb mutants but in the review article by Ando et al (PMID: 34685412) it is stated that "indicating that endothelial cells can produce basic barrier integrity without pericytes in zebrafish."*

We thank the reviewer for their comments and pointing out literature that we had not cited (this has been corrected in our revised manuscript).

As noted by other reviewers, our study goes beyond simply confirming previous literature. The quoted section by the reviewer from Ando et al 2021 regarding intact barrier integrity in *pdgfrb* mutants is a conclusion based on apparent lack of haemorrhages in *pdgfrb* mutants[1]. Our work shows haemorrhages in older animals and as such is in line with these previously published results, but it also extends previous work, for the first time reporting detailed functional analysis to assess BBB integrity. Our study uses definitive tracer assays (now including extensive revisions) to identify intact the BBB in *pdgfrb* mutants in live animals. This has not been previously described and is important because it offers a new perspective on the evolutionary conservation (or otherwise) of pericyte control of BBB function. Furthermore, our study investigates the nature of hotspot leakage and haemorrhages in more detail than in previous work.

> *Weaknesses:*
>
> *(1) The authors should avoid using violin plots, which show distribution. Instead, they should replace all violin plots in the figures with graphs showing individual data points and standard deviation. For Figure 2f specifically, the standard deviation in the analyzed cohort should be shown.*

This is a good point and we have replaced the violin plots with individual data points and shown all data as mean±SEM.

> *(2) The authors have not shown the reduced PDGFRB protein or the effect of mutation on mRNA level in their zebrafish mutant.*

Our *pdgfrb*^{uq30bh} mutant allele introduces a mutation predicted to generate a truncated protein very similar to previously validated alleles (see detail in revised Extended Data Fig. 1a and methods). Our *pdgfrb*^{uq30bh} mutant also phenocopies previous *pdgfrb* mutants (*sa16389* and *um148* alleles)[2,3], displaying mural cell loss with multiple markers (Fig. 1a, new data in Extended Data Fig. 1b–c, Fig. 3b–c; Extended Data Fig. 4c–d) and the same typical morphological defects and survival rates (new data in Extended Data Fig. 1d–f). Thus our mutant phenocopy gives confidence it is most likely a null allele, in line with previous papers studying presumed null alleles[1].

We believe this provides sufficient confidence in this allele of *pdgfrb*. Moreover, considering that our manuscript focusses on loss of mural cells and we show definitively that this mutant has robust loss of mural cells in the brain, our mutant is suitable for this study.

> *(3) Statistical data analysis: Did the authors perform analyses to investigate whether the data has a normal distribution (e.g., Figures 1d, e)?*

We thank the reviewer for raising this and apologise for this oversight. All data have now been assessed for normality using Shapiro-Wilk test and further statistical analyses have been performed accordingly. The specific quantifications referred to by the reviewer in Extended Data Fig. 3a–d (previously Fig. 1d-e), have normal distribution except for quantification measuring 70 kDa extravasation at 7 dpf, therefore Mann-Whitney test has been used for this comparison. Further information can be found in figure legends and methods.

> *(4) Analysis of tracer extravasation. The use of 2000 kDa dextran intensity as an internal reference is problematic because the authors have not provided data demonstrating that the 2000 kDa dextran signal remains consistent across the entire vasculature. The authors have not provided data demonstrating that the 2000 kDa dextran signal in vessels exhibits acceptable variance across the vasculature to serve as a reliable internal reference. The variability of this signal within a single animal remains unknown. The presented data do not address this aspect.*

We thank the reviewer for their comment and agree that analysis was needed for showing 2000 kDa dextran as a reliable normalization signal.

We now show the data in the following Figures that demonstrate the consistency of signal throughout the vasculature using this 2000-kDa tracer: Extended Data Fig. 2b, Extended Data Fig. 3a and c, Extended Data Fig. 5a, Extended Data Fig. 6. In fact, we observe that this 2000 kDa tracer provides a very reliable marker of large and small calibre vessels in larval, juvenile and adult animals, even in fixed and cleared whole tissues and animals (e.g. Extended Data Fig. 2d-e, Extended Data Fig. 5 and 6).

Our further experiments and analysis support the use of this tracer as an ideal way to normalise for variation between animals and coupled with improved masking of vessels using transgenic labels (e.g. Extended Data Fig. 2b) we can quantify across whole vascular networks to reduce the concern about variation within individual animals. We also find 2000 kDa shows negligible leakage through the brain vessels Extended Data Fig. 2b–c (new data) at 2 hours post-injection (hpi) and provided images in Extended Data Fig. 6b–b'' showing detectable signals even at 6 hpi. Finally, results generated with this approach, normalisation to transgenic markers or even raw parenchymal values of tracer intensity, generate the same conclusions. In addition, we point the reviewer to a recent pre-print that further validates this method from our team[4].

Overall, we find the use of this tracer an ideal way to normalise for differences in injection volumes between animals and we recommend the use of this method to other groups assessing BBB leakage in zebrafish.

> *Additionally, it's intriguing that the signal intensity in the parenchyma of the tested tracers presents a substantial range, varying by 20-30% in the analysed cohort (Figure 1g, Extended Figure 1e). Such large variability raises the question of its origin. Could it be a consequence of the normalization to 2000 kDa dextran intensity which differs between different fish? Or is it due to the differences in the parenchymal signal intensity while the baseline 2000 kDa intensity is stable? Or is the situation mixed?*

This is a good point raised by the reviewer.

To address this, we have used the following approaches:

(1) We provide additional experiments and normalisation methods that support the utility of our tracer studies (new data in Fig 2a–f and Extended Data Fig. 2b–c), discussed in detail below.

(2) We provide graphs of the raw parenchymal distribution of tracer not normalised at all (also requested by reviewer 1). This is provided in Author response image 1 and further supports all our conclusions, showing that our normalisation methods generate meaningful data.

Overall, the range of parenchymal intensity that we see after tracer injection and live imaging shows variations introduced during microinjection. However, these ranges are in-line with previous publications using similar methods (see studies by O'Brown et al 2019 and

2023)[5,6], allow reliable statistical comparisons to be drawn between control and mutants and allow us to detect both immature and functional BBB states during zebrafish development (new data in Fig. 2e-f).

Of note, the variability we see is likely introduced during the injection process into tiny larval blood vessels and is the reason why we perform normalization of parenchymal tracers to a vascular dextran signal that doesn't leak from brain vessels. In our studies, 2000-kDa dextran has been co-injected with the smaller size tracers, therefore any potential differences in injection volumes as well as imaging conditions (however consistent) should be reduced by this method.

> *An alternative and potentially more effective approach would be to cross the pdgfrb mutant line with a line where endothelial cells are genetically labeled to define vessels (e.g. the line kdrl used in acquiring data presented in Figure 2a). Non-injected controls could then be used as a baseline to assess tracer extravasation into the parenchyma.*

We thank the reviewer for this suggestion.

In response, we have performed new tracer leakage experiments at 7 and 14 dpf in siblings and pdgfrb mutants and quantified parenchymal tracer extravasation by normalizing to vascular reporters (*Tg*(*kdrl:EGFP*)^{s843} or *Tg*(*kdrl:Hsa.HRAS-mCherry*)^{s916}). The results were in-line with the previously presented and independent experiments and showed indistinguishable phenotypes between siblings and pdgfrb mutants (new data, Fig. 2a–d). We also used uninjected controls to assess baseline and saw consistent values approaching zero in these images and did not include this in the revised paper.

Furthermore, we have also used this approach in wild-type larvae at 3 dpf (immature BBB) and 7 dpf (functional BBB)[5]. We detected significantly higher parenchymal extravasation of 10 and 70 kDa tracers at 3 dpf compared to 7dpf, demonstrating that our method can detect leakage (new data, Fig. 2e–f).

We believe that both normalization approaches have advantages (as discussed above), therefore showing the same results with these two different approaches has further strengthened our findings.

> *How is the data presented in Figure 3e generated? How was the dextran intensity calculated? It looks like the authors have used the kdrl line to define vessels. Was the 2000 kDa still used as in previous figures? If not, please describe this in the Materials and Methods section.*

We have moved this data to Fig. 4e (previously Fig. 3e).

Previously, we had plotted raw data due to the nature of the experiment being conducted on a vibratome sectioned tissue. The 2000 kDa tracer was not used. In response to this query and to be consistent with the new approach suggested by the reviewer, we have revised the quantification by normalizing the 10 kDa tracer extravasation to *Tg*(*kdrl:Hsa.HRAS-mCherry*)^{s916}) for this and the new experiments on juveniles (Fig. 5h–i). Please see the corresponding figure legends or revised methods (lines 464–472).

> *(5) The authors state that both controls and mutants show extravasation of 1 kDa NHS-ester into the parenchyma. However, the presented images do not illustrate this; it is not obvious from these images (Extended Data Figure 1c). Additionally, the presented quantification data (Extended Data Figure 1e) do not show that, at 7 dpf, the vasculature is permeable to this tracer. Note that the range of signal intensity of the 1 kDa NHS-ester is similar to the 70 kDa dextran (Figure 1g and Extended Figure 1e). Would one expect an increase in the ratio in case of extravasation, considering that the 2000 kDa dextran has the same intensity in all experiments? Please explain.*

We thank the reviewer for raising this important point.

To clarify, we have never claimed that "2000-kDa dextran has the same intensity in all experiments". On the contrary, vascular 2000 kDa normalization has been used to account for potential differences caused by injection, as stated in the submitted supplementary materials and now made more clear in the revision.

In response to this query, we conducted more detailed analysis on tracer extravasation patterns based on molecular weight (new data, Extended Data Fig 2b–c). This analysis showed that 1- and 10-kDa tracers have much higher extravasation rate compared to 70- and 2000-kDa tracers. Interestingly, we did not find a significant difference between 1 and 10 kDa extravasation. Therefore, in the revised manuscript we used only 10 kDa in further experiments and have removed 1 kDa from the figures.

To assess the tracers individually (new data in Extended Data Fig. 2c), parenchymal extravasation of individual tracers was normalised to their own vascular signal (eg. Mean intensity of 10 kDa in midbrain/mean intensity of 10 kDa in vasculature), to account for potential differences in injection volume. This provides a suitable method to assess leakage in wild-type animals and is now in line with how previous studies have analysed such tracer injections[5,6]. Please see revised figure legends and supplementary materials for details.

> *(6) The study would be strengthened by a more detailed temporal analysis of the phenotype. When do the aneurysms appear? Is there an additional loss of VSMC?*

We thank the reviewer for this suggestion, and we have now performed staged imaging of the pdgfrb mutants and siblings between 7 and 21 dpf using *TgBAC*(*acta2:EGFP*)^{uq17bh} transgene (new data, Fig. 3b-c; Extended Data Fig. 4a–d). Consistent with previous results, *acta2:EGFP*-positive cells surrounding the middle mesencephalic central arteries (MMCtA) were missing in pdgfrb mutants. At 21 dpf, we have also observed a mild dilation of these vessels, likely the earliest changes to generate aneurysms (new data, Fig. 3c).

To extend the number of stages analysed in this study, we have also performed new tracer leakage experiments in juveniles (30 dpf) and found that aneurysms can be detected at this age when the 10 kDa tracer is used (new data in Fig. 5b–b'). Consistent with the adult stage phenotype, aneurysms were limited to the larger calibre vessels (arteries) in the brain. We have also observed hotspots, and upon quantification, we found fewer numbers in juveniles compared to adults, suggesting that severity of aneurysms and hotspots increase with age.

Taken together, our results show that the aneurysms in *pdgfrb* mutants start appearing at late larval/early juvenile stages (~21 dpf) with observable dilations. By 30 dpf, aneurysms accompanied by small numbers of hotspots are observed, which exhibits significantly increased numbers by adulthood. This also correlates with reduced development and survival rate of *pdgfrb* mutants after 30 dpf (new data, Extended Data Fig. 1d–e).

> *(7) The authors intended to analyze the BBB at later stages (line 128), but there is not a significant time difference between 2 months (Figure 2) and 3 months (Figure 3) considering that zebrafish live on average 3 years. Therefore, the selection of only two time-points, 2 and 3 months, to analyze BBB changes does not provide a comprehensive overview of temporal changes throughout the zebrafish's lifespan. How long do the pdgfb mutants live?*

Respectfully, zebrafish transition from juvenile stages to adulthood between 2 and 3 months and there are many significant differences in the physiology of this organism at these two ages. At 2 months, zebrafish are still juveniles undergoing metamorphosis with rapid growth and ongoing skeletal and vascular development. By 3 months, they are sexually mature adults and have much more developed cranioskeletal and vascular systems. Having said that,

we take the reviewers important point that further temporal resolution would improve the study.

We have performed new experiments in 1-month-old animals and provided comprehensive analysis of the vascular phenotypes occurring in *pdgfrb* mutants. These were very informative experiments analysing leakage using 10-kDa tracer injections and have significantly improved the study. We had previously provided experiments at 5-month-old adults as well (previously Fig. 4a–b and Extended Data Fig. 4a) and so now the study includes larval stages (7, 14 dpf), juveniles at 1 and 2 months and adults at 3 and 5 months. While the additional timepoints did not offer up any new conclusions, they significantly enhanced the body of work overall.

Of further note, we provided survival data up to 90 dpf where survival of the *pdgfrb* mutants is significantly reduced compared to siblings (Extended Data Fig. 1e). We believe this is associated with the severity of the aneurysms and haemorrhages which probably lead to lethality in these mutants.

> *(8) Why is there a difference in tracer permeability between 2 and 3 months (Figures 2 and 3)? Are hemorrhages not detected in 2-month-old zebrafish?*

In response to this and other queries, we have added new additional experiments that provide more detailed temporal analysis on tracer accumulation (new data in Fig. 5b–c, Fig. 5f–g).

In short, we do not see obvious haemorrhages in 1- or 2-month fish at a gross level during dissections (not shown). We find that using 10-kDa tracer, we can detect small hotspots at aneurysms as early as 1 month, likely representing the earliest loss of integrity. We do not see obvious hotspots in 2-month-old animals when we use the 70-kDa tracer, this suggests to us that it is less sensitive for hotspot detection (in line with new Extended Data Fig. 2c). Finally, we find that the number of hotspots increases dramatically from Juvenile to Adult stages in our datasets, which we take as indicative of a progressive phenotype.

Overall, tracer size matters for detecting hotspots and they become more apparent in older animals - we have added a note in the main text to cover these points (lines 200–205)

> *(9) Figure 3: The capillary bed should be presented in magnified images as it is not clearly visible. Figure 3e shows that in the pdgfb mutant the dextran intensity is higher also in regions 6-10. How do the authors explain this?*

We thank the reviewer for raising this important point.

Firstly, we now include enlarged views of the capillary beds for this experiment (Fig. 4d') and new experiments mentioned below.

Secondly, in relation to why there is higher tracer in lateral locations and not just medial sites of haemorrhage, we believe that this is most likely due to the progressive spread of tracer from the medial hotspots. To test if this is likely, we performed additional experiments and tested tracer accumulation at 2 different timepoints in brains collected at 0.5 or 6 hpi (new data in Fig. 5f–g, Extended Data Fig. 6a–b''). Tracer accumulation at 0.5 hpi was very minimal and was primarily limited to hotspots and nearby regions new data in (Fig. 5h), whereas a higher tracer accumulation in brains was observed across medial to lateral regions at 6 hpi (new data in Fig. 5i) in *pdgfrb* mutants. Comparing the data in Figure 4 (2 hpi) and new data in Figure 5i (6 hpi), the 10 kDa-tracer appears to have spread to more lateral locations given the increased time allowed post injection.

We cannot formally exclude the possibility that tracer leakage does occur slower through capillaries than at major hotspots, which might fit with the proposed model of slow leakage

via increased EC transcytosis[7-9]. However, considering that we cannot detect increased tracer accumulation in *pdgfrb* mutants that lack aneurysms and haemorrhages at 7 and 14 dpf, such a scenario would require capillary transcytosis to be active at later juvenile and adult stages but not in larval and late larval animals. Thus, we believe the most plausible explanation is that aneurysm/haemorrhage associated leakage is the primary cause of the vascular integrity defects in zebrafish *pdgfrb* mutants.

We have added discussions addressing this in the revised manuscript (lines 220–230, 300–302).

> *(10) In general, the manuscript would benefit from a more detailed description of the performed experiments. How long did the tracer circulate in the experiments presented in Figures 2, 3, and 4?*

We thank the reviewer for this suggestion and have now ensured that this is clearly described for in figure legends and methods (lines 391–395).

> *(11) How do the authors explain the poor signal of the 70 kDa dextran from the vasculature of 5-month-old zebrafish presented in Extended Data Figure 3?*

We agree that the dextran signal was reduced compared to the other experiments in that Figure. This is likely due to sample preparation and clearing causing reduced fluorescence. Upon consideration of the presented data and the additional experiments using 10 kDa tracers providing further validations for our claims, we decided to remove this data from the paper.

> *(12) The study would benefit from a clear separation of the phenotypes caused by the loss of VSMC. The title eludes that also capillaries present hemorrhages which is not the case. How do vascular mural cells differ from mural cells? Are there any other mural cells?*

We take the reviewers point and have now updated the title as "Mural cells protect the adult brain from haemorrhage but do not control the blood-brain barrier in developing zebrafish."

> *(13) I have a few comments about how the authors have interpreted the literature and why, in my opinion, they should revise their strong statements (e.g., the last sentence in the abstract).*
>
> *Scientists have their own insights and interpretations of data. However, when citing published data, it should be clearly indicated whether the statement is a direct quote from the original publication or an interpretation. In the current manuscript, the authors have not correctly cited the data presented in the two published papers (references 5 and 6). These papers do not propose a model where pericytes suppress "adsorptive transcytosis" (lines 73-76). While increased transcytosis is observed in pericyte-deficient mice, the specific type of vesicular transport that is increased or induced remains unknown.*
>
> *Similarly, lines 151-152 refer to references 5 and 6 and use the term "adsorptive transcytosis," but the authors of both papers did not use this term. Attributing this term to the original authors is inaccurate. Additionally, lines 152-153 do not accurately represent the findings of references 5 and 6. These papers do not state that there is an induction of "caveolae" in endothelial cells in pericyte-deficient mice. In the absence of pericytes, many vesicles can be observed in endothelial cells, but these vesicles are relatively large. It is more likely that there is some form of uncontrolled transcytosis, perhaps micropinocytosis. Please refer to the original papers accurately.*

We thank the reviewer for these comments. We take the point and have rewritten the manuscript carefully to improve accuracy and avoid misrepresenting any previous claims made in specific papers.

> *Also, the authors have missed the fact that in mice, the extent of pericyte loss correlates with the extent of BBB leakage. To a certain extent, the remaining pericytes, can compensate for the loss by making longer processes and so ensure the full longitudinal coverage of the endothelium. This was shown in the initial work of Armulik et al (reference 5) and later in other studies.*

We certainly did not miss this important point (as we are also working with these mouse models) and we now include reference to this in our expanded discussion. Of note, we do think it would be worthwhile assessing if the extent of BBB leakage and pericyte coverage also correlates with the presence of microhaemorrhages in these hypomorphic mouse models, although this is more challenging to do in mice than in zebrafish.

> *The bold assertion on lines 183 -187 that a lack of specific BBB phenotype in pdgfrb zebrafish mutant invalidates mouse model findings is unfounded. Despite the notion that zebrafish endothelium possesses a BBB, I present a few examples highlighting the differences in brain vascular development and why the authors' expectation of a straightforward extrapolation of mouse BBB phenotypes to zebrafish is untenable.*
>
> *In mice Pdgfrb knockout is lethal, but in zebrafish, this is not the case. In marked contrast to mice, however, zebrafish pdgfrb null mutants reach adulthood despite extensive cerebral vascular anomalies and hemorrhage. Following the authors' argumentation about the unlikely divergence of zebrafish and mice evolution, does it mean that the described mouse phenotype warrants a revisit and that the Pdgfrb knockout in mice perhaps is not lethal? Another example where the role of a gene product is not one-to-one, which relates to pericyte development, is Notch3. Notch3-null mice do not show significant changes in pericyte numbers or distribution, suggesting a less prominent role in pericyte development compared to zebrafish.*
>
> *Although many aspects of development are conserved between species, there are significant differences during brain vascular development between zebrafish and mice. These differences could reveal why the BBB is not impaired in zebrafish pdgfrb mutants. There is a difference in the temporal aspect when various cellular players emerge. The timing of microglia colonization in the brain differs. In mice, microglia colonization starts before the first vessel sprouts enter the brain, while in zebrafish, microglia enter after. Additionally, microglia in zebrafish and mice have a different ontogeny. In mice, astrocytes specialize postnatally and form astrocyte endfeet postnatally. In zebrafish, radial glia/astrocytes form at 48 hpf, and as early as 3 dpf, gfap+ cells have a close relationship with blood vessels. Thus, these radial glia/astrocyte-like cells could play an important role in BBB induction in zebrafish. It's worth noting that in Drosophila, the blood-brain barrier is located in glial cells. While speculative, these cells might still play a role in zebrafish, while the role of pericytes does not seem to be crucial. Pericytes enter the brain and contact with developing vasculature (endothelium) relatively late in zebrafish (60 hpf). In mice, the situation is different, as there is no such lag between endothelium and pericyte entry into the brain. I suggest that the authors approach the observed data with curiosity and ask: Why are these differences present? Are all aspects of the BBB induced by neural tissue in zebrafish? What is the contribution of microglia and astrocytes?"*
>
> *Another interesting aspect to consider is the endothelial-pericyte ratio and longitudinal coverage of pericytes in the zebrafish brain, and how this relates to what is observed in mice. How similar is the zebrafish vasculature to the mouse vasculature when it comes to*

> *the average length of pericytes in the zebrafish brain? Does the longitudinal coverage of pericytes in the zebrafish brain reach nearly 100%, as it does in mice?*
>
> *Based on the preceding arguments, it is recommended that the authors present a balanced discussion that provides insightful discussion and situates their work within a broader framework.*

Overall, we agree with most of the points made by the reviewer above. As we have now extended the format of this paper to be a full article, we have space to provide an extended discussion and introduction. We now try to capture many of the points made by the reviewer and we think that this has significantly improved the paper. We thank the reviewer for this contribution.

We do want to point out that we did not state that our findings using zebrafish pdgfrb mutants invalidate mouse model findings. We suggest that a deeper analysis to understand the nature of the hotspots in mural cell deficient mammalian models could be very interesting in light of the zebrafish observations. We hope that the revised discussion better reflects this.

> ***Reviewer #3 (Public review):***
>
> *This manuscript examines the role of pdgfrb-positive pericytes in the establishment and maintenance of the blood-brain barrier (BBB) in the zebrafish. Previous studies in PDGFB- or PDGFRB-deficient mice have suggested that loss of pericytes results in disruption of the BBB. The authors show that zebrafish pdgfrb mutant larvae have an intact BBB and that pdgfrb mutant adult fish show large vessel defects and hemorrhage but do not exhibit substantial leakage from brain capillaries, suggesting loss of pericytes is not sufficient to "open" the BBB. The authors use beautiful and compelling images and rigorous quantification to back up most of their conclusions. The imaging of the adult brain is particularly nice. The authors rigorously document the lack of BBB leakage in pdgfrbuq30bh mutant larvae and large vessel phenotypes (eg, enlargement and rupture) in pdgfrbuq30bh mutant adults. A few points would help the authors to further strengthen their findings contradicting the current dogma from rodent models.*

We appreciate the reviewer's comments on the manuscript overall and agree that addressing the raised points was needed to strengthen our findings. We have addressed the main points below and believe that this revision greatly improves this study.

> *Major point:*
>
> *The authors document pericyte loss using a single TgBAC(pdgfrb:egfp)ncv22 transgenic line driven by the promoter of the same gene mutated in their pdgfrbuq30bh mutants. Given their findings on the consequences of pericyte loss directly contradict current dogma from rodent studies, it would be useful to further validate the absence of brain pericytes in these mutants using one of several other transgenic lines marking pericytes currently available in the zebrafish. This could be done using pdgfrb crispants, which the authors show nicely phenocopy the germline mutants, at least in larvae. This would help nail down the absence of any currently identifiable pericyte population or sub-population in the loss of pdgfrb animals and substantially strengthen the authors' conclusions.*

We thank the reviewer and agree that examination of *pdgfrb*^{uq30bh} mutants using another transgenic line labelling pericytes would further validate the absence of brain pericytes. We generated a transgenic line, *TgBAC*(*abcc9:abcc9-T2A-mCherry*)^{uom139}, to visualise pericytes and validated the absence of brain pericytes in the *pdgfrb* mutants (revised Extended Data Fig. 1b). The loss of brain pericytes matched our findings using *TgBAC*(*pdgfrb:egfp*)^{uq15bh} line as well as previously published data by Ando et al 2016-2021, where the brain pericytes except for metencephalic artery were missing[2,3].

> *Other issues:*
>
> *The authors should provide more information about the pdgfrbuq30bh mutant and how it was generated (including a diagram in a supplemental figure would be useful).*

We thank the reviewer for this suggestion. In addition to the explanations provided in supplementary materials, we have added a schematic, provided sanger sequencing results showing the mutation as well as predicted effect of the mutation on the protein domains (Extended Data Fig. 1a).

> *It would be helpful to show some data on whether mutants show morphological phenotypes or developmental delay at 7 and 14 dpf, to provide some context to better assess the reduced branching and vessel length vascular phenotypes (see Figures 1c-e).*

We thank the reviewer for this suggestion. We have provided further details on body length and survival of the *pdgfrb* mutants until 90 dpf. As reported by Ando et al 2021, we did not observe any distinguishing feature until about 30 dpf[1,3]. The adult anatomy of our mutant allele matches that of previously described null mutants and is now shown (Extended Data Fig. 1f).

> *If available, it would be helpful to have a positive control for the tracer leakage experiments - a genetic manipulation that does cause disruption of the BBB and leakage at 2 hours post-tracer injection (see Figures 1f and g).*

We thank the reviewer for this suggestion and agree that a positive control would validate reliability of our method. We have performed new experiments at 3 dpf when BBB integrity is not yet established and at 7 dpf when BBB is functional in zebrafish[5], testing both 10 and 70 kDa tracers (new data in Fig. 2e–f). We detected significantly higher tracer accumulation at 3 dpf, showing that our methods can detect tracer leakage in the brain.

> *Quantification of the findings in Figure 4c, d would be useful, as would the use of germline fish for these experiments if these are now available. If this is not possible, it would be helpful to document that the crispants used in these experiments lack pdgfrb:egfp pericytes at adult stages (this is only shown for 5 dpf larvae, in Extended Data Figure 4b).*

We thank the reviewer for this comment. Using *TgBAC(pdgfrb:egfp)*^{uq15bh} line, we have imaged coronal brain sections collected from 10-week old pdgfrb crispants and uninjected siblings (age-matched animals used in Fig. 5d–e, previously Fig. 4c–d). We have now included data showing that adult pdgfrb crispants lack brain mural cells, phenocopying *pdgfrb*^{uq30bh} mutants (new data, Extended Data Fig. 6f). These particular crispants are very reliable in our hands and nicely reproduce stable mutant phenotypes, giving us confidence to use the faster F0 approach in this experiment.

> *Adult mutants clearly show less dye leakage in the more superficial capillary regions than WT siblings, but dextran intensity is a bit higher, although this could well be diffusion from more central brain regions where overt hemorrhage is occurring. Along similar lines though, the authors' TEM data in Extended Data Figure 4d hints that there may be more caveolae in mutant brain capillaries, although the N number was lower here than for the measurements from TEM of larger central vessels (Figure 4g). It would be useful to carry out additional measurements to increase the N number in Figure 4d to see whether the difference between wild-type sibling and mutant capillary caveolae numbers remains as not significant.*

We thank the reviewer for these raising important points and suggestions.

Firstly, in relation to signal in capillary regions and likely diffusion from hotspots, please see the response to reviewer 3 point 9 above.

Secondly, we have imaged and analysed more capillaries in both *pdgfrb* mutants and siblings (Extended Data Fig. 7a–b, previously Extended Data Fig. 4d). The results showed no significant difference between these groups, suggesting that capillary EC transcytosis is unchanged in our *pdgfrb* mutants.

> *It might be helpful to include some orienting labels and/or additional descriptions in the figure legends to help readers who are not used to looking at zebrafish brain vessels have an easier time figuring out what they are looking at and where it is in the brain.*

We thank the reviewer for this suggestion and agree that adding further information in the figure legends and illustrations about orientation would make it easier for readers. In addition to the information provided in the figure legends in the submitted version, we have added an illustration, more labels on the revised figures, extended the descriptions in figure legends, main text and methods.

We have added a schematic depicting the tracer leakage assay workflow, orientation of live imaging and analysed region of interest (Extended Data Fig. 1a–b).

All figure legends have been updated with the anatomical position and microscopy view.

Additional labels on figures have been added to understand the referenced vessel names (new data in Fig. 3c and Extended Data Fig. 4a–b').

> ***Recommendations for the authors:***
>
> ***Reviewer #1 (Recommendations for the authors):***
>
> *The study uses the intensity of tracer signals within the vessels to analyze BBB permeability, potentially underestimating leakage severity. The dye intensity is measured 2 hours after injection, however, other studies have already observed leakage after 30 Minutes, by imaging directly in the brain parenchyma. The overall intensity should also decrease through leakage from the other vessels of the body, e.g. in the trunk and tail. Probably the loss of intra-vascular dye intensity from leakage in barrier-free vessels is already so high (after 2 hours) that the smaller amount of leakage across the BBB cannot be observed.*

We thank the reviewer for this comment and suggestion. We agree that small sized tracers leak from vasculature, particularly through fenestrated vessels in the trunk and tail. We have based our timing on previous studies and our own experience. In zebrafish, the study by O'Brown et al 2019 also used 2 hpi[5] for detection of leakage in *mfsd2aa* mutants, which also has been proposed to regulate BBB integrity by controlling EC transcytosis. Therefore, we believe that performing experiments at 2 hpi is appropriate to investigate roles of pericytes in BBB integrity. Our data would suggest that this timing works.

In response to this and other comments, we performed further experiments and analyses to test leakage of tracers testing molecular weights ranging from 1 to 2000 kDa individually. We showed that these tracers can reliably be detected in brain parenchyma and vasculature when imaged at 2 hpi. In another study, we showed that medium size tracers such as 40 kDa Dextran can be reliably detected in the vasculature in similar timepoints[10]. Considering we have performed experiments using 10 and 70 kDa tracers do detect parenchymal tracer accumulation and tracer still within the vessels, we believe this timepoint is appropriate for assessing BBB integrity in zebrafish.

In addition to these experiments, see our tracer leakage experiments in 1-month-old animals, at 0.5 and 6 hpi to test leakage pattern described above (Fig. 5 and Extended Data Fig. 6).

> *Therefore, the authors will need to validate their method of choice, showing an impairment of the BBB, caused by other agents (known to affect the BBB), and at 48hpf, when the BBB is not tightened yet. One example for BBB impairment can be found in O'Brown et al (2019), eLife 8e47326. doi: 10.7554/eLife.47326*

We thank the reviewer for this suggestion. As shown by O'Brown et al 2019, we have performed experiments at 3 dpf when BBB integrity is not mature and at 7 dpf when BBB is functional[5], testing both 10 and 70 kDa tracers. We detected significantly higher tracer accumulation at 3 dpf, showing our new additional method (see below) can detect tracer leakage in the brain (new data in Fig. 2e–f).

> *Ideally, the authors would also supplement the method with additional approaches in the younger developmental stages to validate their findings.*
>
> *The validation of the method and the findings is particularly important for the claims of lack of BBB impairment in the absence of mural cells, as this is a "negative" finding.*

In response to this and comments from other reviewers, we performed additional tracer leakage experiments (new data in Fig. 2a–d) where we imaged 10 and 70 kDa tracers with a vascular reporter (*Tg*(*kdrl:EGFP*)^{s843} or *Tg*(*kdrl:Hsa.HRAS-mCherry*)^{s916}) and used this reporter for normalisation. Both this approach as well as the experiments provided in the first submission (updated as Extended Data Fig. 3a–d) showed that *pdgfrb* mutants at 7 and 14 dpf have indistinguishable BBB integrity compared to siblings. See also Author response image 1 that further addresses this.

> *I also strongly suggest to rephrase and downtown the claim that vascular mural cells do not control the blood-brain barrier in developing zebrafish.*
>
> *As a negative finding cannot be proven completely and lots of the previously shown effects on murine BBB impairment are rather weak (when caused by single agents such as Claudin5 deficiency or Sphingosine-phosphate receptor1 knockout), it might be important to only claim that in zebrafish no strong impairment (as observed in the mural cell-deficient mouse) could be observed. Or rephrase it to "no impairment as severe as/comparable to ... could be observed" and then provide an impairment control for the developmental stages.*

We thank the reviewer for this comment and agree that negative findings are very challenging to prove. However, we find no evidence of leakage of the BBB in animals lacking mural cells at 7 and 14 dpf and believe that our data is robust on this point. As such, we believe we show that a vertebrate with a largely conserved EC BBB, can have intact barrier function in the absence of mural cells.

We have as suggested revised our claims throughout the manuscript to provide more further nuanced discussion of this, but we do not want to water down our claims too much as we believe they are important. We hope that the reviewer will appreciate our carefully worded and expanded discussion section.

> *Additional items of interest to the readers and therefore suggestions to improve the manuscript could be*

> *(1) To include more molecular analysis: while the study identifies caveolae induction and basement membrane thickening as potential contributors to focal leakage, the exact molecular mechanisms linking mural cell loss to these structural changes are not deeply investigated.*
>
> *(2) Also, the study primarily associates BBB disruption in the adult with aneurysms. Therefore other subtle or diffuse changes to BBB permeability that might occur even without overt vascular lesions are potentially underrepresented.*
>
> *However, following up experimentally on these might exceed the scope of the manuscript.*

We thank the reviewer for these suggestions and agree with both points. However, as stated by the reviewer, these experiments are beyond the scope of the manuscript and represent future directions for our lab and others.

> ***Reviewer #2 (Recommendations for the authors):***
>
> *(1) Mouse genes should be written as follows: Pdgfb, Pdgfrb and be in italics. See line line 70: it should be written "Pdgfb and Pdgfrb (italics)" and not "PdgfB and Pdgfrβ".*

We have updated the text according to the reviewer's suggestion.

> *(2) Please state the age of the fish analyzed in Figure 1f and 1g.*

We have moved this data to Extended Fig. 3a–d (previously Fig. 1f-g) and have placed age information on the images and in the figure legends.

> *(3) Is the reduced vascular complexity in pdgfb mutant due to reduced angiogenesis or due to excessive pruning?*

This is a good question, and we do not know at this stage. We have unpublished data that suggest pericytes secrete angiogenic growth factors, but this question warrants a thorough investigation that we believe is beyond the scope of this current study.

> *(4) Please check that the figure legends state the correct number of fish analysed. For example, Figure 1 d, e N=8 but there seem to be 9 data points per group - 14dpf.*

We apologise for this mistake and thank the reviewer for raising this. We have updated the graphs and figure legends accordingly.

> *(5) Please indicate in the figures the genotypes (wt, het) of a sibling presented alongside a pdgfb mutant.*

Wild-type and heterozygous mutants are commonly used together in zebrafish research as a collective control group termed siblings. Since we didn't see any difference between wild-type and *pdgfrbuq30bh/-* groups in any experiments, we reported these groups together. This is now stated in the supplementary materials.

One exception to this was examination of the growth and survival rates where we show the genotypes separately (new data in Extended Data Fig. 1b-f).

> *(6) Please explain clearly what region is shown in Figure 2B. I do not understand the explanation "approximate location of dotted line". Is the image in the panel "a" top view of a brain?*

We have moved this data to Fig. 3a' (previously Fig. 2b) and replaced the dotted line in Figure 3a (previously Fig. 2a) with a white box indicating the location of the restricted region in the

whole brain image.

We have revised the text as below:

“Subset of z-slices from the whole brain imaging in (a) and (b) (white boxes) indicating mural cell loss and abnormal capillary network patterning. 100-µm-thick maximum intensity projections (MIP) were generated using the continuation of the left middle mesencephalic central artery (MMCtA, arrow) as an anatomical landmark.”

In addition, we have updated all our figure legends clearly stating the view and anatomical position of the imaged sample.

> *(7) Figure 2e: Note that- the dotted areas do not correspond to the areas magnified. Please adjust.*

We have moved this data to Extended Data Fig. 5a (previously Fig. 2e–e') and updated the location of the white box in 5a shown in enlarged view in 5a'.

> *(8) Lines 112 and 114 - Should the indicated figure be Figure 2b-d and Figure 2c-d, respectively, and not Figure 1?*

We thank the reviewer for pointing out this mistake. All the figure legends are now referred to appropriately in the revised manuscript.

> *(9) Data presented in Figure 2 and Figure 3 can be consolidated and presented as one Figure.*

We thank the reviewer for this suggestion. After addition of new data and revising the manuscript we have decided to keep these data presented separately.

> *(10) Note that Figure 2a,b shows 5-month-old fish, not 2-month-old fish. Additionally, Extended Data Figure 3 shows 5-month-old fish, not 3-month-old fish.*

The stages noted by the reviewer were correctly indicated.

> *(11) Figure 2d: Please clarify the definition of a "large vessel".*

We have observed normal morphology in capillaries and noted aneurysms and hotspots in large calibre vessels such as arteries, which become more severe over time. We have revised this across the manuscript accordingly.

> *(12) Figure 4a, b: Please explain how the hotspots of leakage were defined based on the extravasated tracer.*

Hotspots of leakage are scored when fluorescent tracer aggregates are clearly observed outside the vessels. Vessel borders were defined using the transgenic lines (*Tg*(*kdrl:EGFP*)^{s843} or *Tg*(*kdrl:Hsa.HRAS-mCherry*)^{s916}). We have added a clear description in the methods section (lines 473–475).

> *Figure 4c: Why were Pdgfrb crispants used and not the mutant line?*

They were used as *pdgfrb* crispants phenocopy the lack of brain mural cells (Extended Data Fig. 5e, previously Extended Data Fig. 4b) and mutant phenotype reliably and for practical reasons, because they allow faster experiments and reduce fish usage.

> *Figure 4e: The magnification of the electron microscopy images does not make it possible to clearly identify caveolae. What was the magnification of the collected images for caveolae analysis? How did the authors ensure that they quantified only caveolae and not other types of vesicles?*

Respectfully, we disagree that the magnification is insufficient as our images were captured and analysed consistent with previous ultrastructural descriptions[11,12]. We based our quantification of caveolae on the size of vesicles observed and define them as circular profiles of less than 100 nm in diameter and were scored as luminal or abluminal based on proximity to each surface membrane (within 500 nm of each surface or in a thin-walled vessel the caveolae closest to each surface) (lines 398–409). Importantly, comparable analyses at similar magnifications have been independently validated in multiple caveola-deficient zebrafish genetic models[4,13]. Interestingly given the reviewers comments above, we do see increased vesicular structures that are larger than caveolae, but we only provide quantification of the caveolae here.

> ***Reviewer #3 (Recommendations for the authors):***
>
> *Congratulations to the authors on their really beautiful imaging and rigorous quantitative documentation of phenotypes - this is a really nicely done study, and could be very important to the field with just a few additional experiments to buttress the key conclusions.*

We thank the reviewer for their kind comments.

> *In addition to the comments noted in the public review, I would only point out that there are two mislabeled call-outs in the text (Lines 112 and 114; says Figure 1, should say Figure 2).*

We thank the reviewer for this point and have now revised the text accordingly.

(1) Ando, K., Ishii, T. & Fukuhara, S. Zebrafish Vascular Mural Cell Biology: Recent Advances, Development, and Functions. Life (Basel) 11 (2021). *https://doi.org/10.3390/life11101041*

(2) Ando, K. et al. Clarification of mural cell coverage of vascular endothelial cells by live imaging of zebrafish. Development 143, 1328-1339 (2016). *https://doi.org/10.1242/dev.132654*

(3) Ando, K. et al. Conserved and context-dependent roles for pdgfrb signaling during zebrafish vascular mural cell development. Dev Biol 479, 11-22 (2021). *https://doi.org/10.1016/j.ydbio.2021.06.010*

(4) Lim, Y. W. et al. Trans-Endothelial Trafficking in Zebrafish: Nanobio Interactions of Polyethylene Glycol-Based Nanoparticles in Live Vasculature. ACS Nano (2026). *https://doi.org/10.1021/acsnano.5c21042*

(5) O'Brown, N. M., Megason, S. G. & Gu, C. Suppression of transcytosis regulates zebrafish blood-brain barrier function. Elife 8 (2019). *https://doi.org/10.7554/eLife.47326*

(6) O'Brown, N. M. et al. The secreted neuronal signal Spock1 promotes blood-brain barrier development. Dev Cell 58, 1534-1547 e1536 (2023). *https://doi.org/10.1016/j.devcel.2023.06.005*

(7) Armulik, A. et al. Pericytes regulate the blood-brain barrier. Nature 468, 557-561 (2010). *https://doi.org/10.1038/nature09522*

(8) Daneman, R., Zhou, L., Kebede, A. A. & Barres, B. A. Pericytes are required for blood-brain barrier integrity during embryogenesis. Nature 468, 562-566 (2010). *https://doi.org/10.1038/nature09513*

(9) Mae, M. A. et al. Single-Cell Analysis of Blood-Brain Barrier Response to Pericyte Loss. Circ Res 128, e46-e62 (2021). *https://doi.org/10.1161/CIRCRESAHA.120.317473*

(10) Lim, Y.-W. et al. A Standardized Protocol to Investigate Trans- Endothelial Trafficking in Zebrafish: Nano-bio Interactions of PEG-based Nanoparticles in Live Vasculature. bioRxiv, 2025.2007.2023.666282 (2025). *https://doi.org/10.1101/2025.07.23.666282*

(11) Parton, R. G. & Simons, K. The multiple faces of caveolae. Nat Rev Mol Cell Biol 8, 185-194 (2007). *https://doi.org/10.1038/nrm2122*

(12) Parton, R. G. & del Pozo, M. A. Caveolae as plasma membrane sensors, protectors and organizers. Nat Rev Mol Cell Biol 14, 98-112 (2013). *https://doi.org/10.1038/nrm3512*

(13) Lim, Y. W. et al. Caveolae Protect Notochord Cells against Catastrophic Mechanical Failure during Development. Curr Biol 27, 1968-1981 e1967 (2017). *https://doi.org/10.1016/j.cub.2017.05.06*

https://doi.org/10.7554/eLife.104061.2.sa0